Defence Research and Development Canada
Recherche et développement pour la défense Canada

DEFENCE R&D DÉFENSE

Moving Target Detection with Along-Track SAR Interferometry

A Theoretical Analysis

Christoph H. Gierull

Defence R&D Canada - Ottawa
TECHNICAL REPORT
DRDC Ottawa TR 2002-084
August 2002

Canada

Moving Target Detection with Along-Track SAR Interferometry

– A Theoretical Analysis –

Christoph H. Gierull
Aerospace Radar and Navigation Section

Defence R&D Canada – Ottawa

Technical Report

DRDC Ottawa TR 2002-084

August 2002

Author

Christoph H. Gierull

Approved by

Chris. McMillan
Head/ARN Section

Approved for release by

Gordon Marwood
Head/Document Review Panel

Abstract

This technical report analyses, theoretically, the capability of ground moving target detection based on the SAR along-track interferometric phase. The probability density function of the interferometric phase is derived for the general case that moving target signals are superimposed upon the stationary clutter. This theoretical analysis is an extension of the known statistics for the clutter-only case. Several target models are proposed that depend on one hand on the spatial dimension of the moving target compared to the multilook resolution cell size, and on the other hand on the backscattering type, i.e., deterministic or random target signal. The derived density functions provide the means to quantify the performance limits (by determining the receiver operating characteristics) for any set of system and target parameters, such as false alarm rate, signal-to-clutter ratios (SCR) and target velocities. Hence, deeper insight is provided into results expected from upcoming SAR/GMTI systems such as the Radarsat2 Modex experiment or the enhanced airborne Aurora CP-140 SpotSAR system.

Résumé

Le présent rapport technique expose une analyse théorique sur la capacité de la détection des cibles mobiles basée sur l'interférométrie longitudinale par radar à antenne synthétique (RAS). La fonction de densité de probabilités de la phase de l'interférogramme est dérivée pour le cas général o les signaux des cibles mobiles se superposent à des fouillis stationnaires. Cette analyse théorique est la continuation statistique du cas o il n'y a que du fouillis. Plusieurs modèles sont proposés selon, d'une part, la dimension spatiale de la cible mobile par rapport à la taille de la cellule de résolution à multiples facettes et, d'autre part, le type de rétrodiffusion (c.-à-d., signaux déterministes ou signaux de cibles aléatoires). Les fonctions de densité dérivées offrent le moyen de quantifier les limites de performance (en déterminant les caractéristiques de fonctionnement du récepteur) pour tout ensemble de paramètres de systèmes et de cibles, tels que le taux de fausse alerte, les rapports signal/fouillis et les vitesses anticipées des cibles. Ainsi, on comprendra mieux les résultats qu'on attend des prochains systèmes RAS/GMTI, notamment de l'expérience sur le Radarsat2 Modex ou le système perfectionné SpotSAR à bord du CP-140 Aurora.

Executive summary

In space-borne and airborne radar surveillance it is desirable to be able to detect military moving targets such as tanks, wheeled vehicles or ships within strong ground clutter. One possible way to achieve this is with Synthetic Aperture Radar Along-Track Interferometry (SAR-ATI), where two channels observe the same scene at different times. For stationary terrain the two channel signals are identical and can be canceled out (clutter suppression) by computing the phase difference, i.e., the interferogram, leaving primarily the moving targets in the differential data.

In the past, SAR-ATI was mainly treated in the context of measurement of sea surface currents, though the capability for sensitive ground moving target indication (GMTI) is obvious. Although the effectiveness of ATI for GMTI has been recently evaluated with measured data from several flight experiments no thorough theoretical discussion has been performed so far. Precise knowledge of the interferogram's phase statistics is crucial for the development of statistically based detector tests for distinguishing the moving targets from the clutter.

The purpose of this technical report is to investigate the probability density function of the SAR interferogram's phase when target signals are superimposed upon the clutter echoes. Depending on the spatial dimension of the moving target compared to the SAR resolution cell size and the backscattering type (i.e., deterministic or random target signal), several models are proposed. The derived density functions for most models are graphically illustrated and numerically confirmed with simulated interferometric SAR data.

This analysis provides the means to quantify the performance limits of future SAR systems for arbitrary sets of system and target parameters, such as false alarm rates, signal-to-clutter ratios (SCR) and anticipated target velocities. Deeper insight can be gained into results expected from upcoming SAR/GMTI systems particularly the Radarsat2 GMTI experiment and the enhanced airborne Aurora CP-140 SpotSAR system.

One remarkable result for a typical space-borne system is that a target, with radial velocity of at least $\cong$ 6 m/s and with signal power at least three times the surrounding background (SCR $\cong$ 5 dB) can be detected

with better than 98% probability whereas, on average, only one false alarm occurs in every 10000 SAR image pixels.

Christoph H. Gierull. 2002. Moving Target Detection with Along-Track SAR Interferometry. DRDC Ottawa TR 2002-084. Defence R&D Canada – Ottawa.

Sommaire

Dans la surveillance au moyen de radars aérospatiaux et aéroportés, il est souhaitable de pouvoir détecter en présence de forts fouillis de sol des cibles mobiles militaires, comme des chars, des véhicules à roues ou des navires. Un moyen possible de le faire est d'avoir recours à l'interférométrie longitudinale par radar à antenne synthétique (RAS), qui permet d'observer la même scène dans deux canaux à des moments différents. En terrain fixe, les signaux des deux canaux sont identiques et il est possible de les annuler (suppression de fouillis) en calculant le déphasage, c'est-à-dire l'interférogramme, ce qui laisse surtout les cibles mobiles dans les données différentielles.

Par le passé, l'interférométrie longitudinale par RAS a été considérée principalement dans le contexte de la mesure des courants de surface en mer, même s'il y a manifestement une capacité d'indication de cibles terrestres mobiles (GMTI) précise. Même si on a récemment évalué l'efficacité de l'interférométrie longitudinale pour la GMTI au moyen de données mesurées lors de plusieurs expériences en vol, il n'y a pas encore eu d'examen théorique approfondi. Il est crucial de connaître avec précision les données des phases de l'interférogramme pour développer des essais de détection fondés sur des statistiques dans le but de distinguer entre les cibles mobiles et le fouillis.

Le présent rapport technique a pour but d'étudier la fonction de densité de probabilités de la phase de l'interférogramme du RAS lorsque les signaux de cibles sont superposés à des échos de fouillis. Selon les dimensions spatiales de la cible mobile par rapport à la taille de la cellule de résolution du RAS et au type de rétrodiffusion (c'est-à-dire des signaux déterministes ou des signaux de cibles aléatoires), plusieurs modèles sont proposés. Les fonctions de densité dérivées pour la plupart des modèles sont illustrées graphiquement et confirmées numériquement par des données simulées de RAS interférométriques.

La présente analyse fournit le moyen de quantifier les limites de performance des futurs systèmes RAS pour des ensembles arbitraires de paramètres de système et de cible, comme les taux de fausse alarme, les rapports signal/fouillis et les vitesses des cibles anticipées. On pourra ainsi mieux comprendre les résultats attendus des prochains systèmes de RAS/GMTI, en particulier ceux qui ressortiront de l'expérience sur le dispositif GMTI de Radarsat 2 et le système amélioré de détection aéroporté SpotSAR à bord

du CP-140 Aurora. Un résultat remarquable pour un système aéroporté type est qu'il est possible de détecter une cible ayant une vitesse radiale d'au moins 6 m/s et un signal d'une puissance d'au moins trois fois le bruit ambiant (rapport signal/fouillis de 5 dB) avec une probabilité supérieure à 98 %, alors qu'en moyenne, il n'y a qu'une seule fausse alarme à tous les 10 000 pixels d'images de RAS.

Christoph H. Gierull. 2002. Détection de cibles mobiles au moyen de l'interférométrie longitudinale par radar à antenne synthétique (RAS) – Analyse théorique –. DRDC Ottawa TR 2002-084. R&D pour la défense Canada – Ottawa.

Table of contents

Abstract i

Résumé i

Executive summary iii

Sommaire v

Table of contents vii

List of figures ix

List of tables xi

Acknowledgements xii

1. Introduction 1

    1.1 Stationary Clutter Model 3

    1.2 Inclusion of Channel Errors and Imbalances 4

2. Deterministic Moving Target Model 7

    2.1 Multiple Movers in Multi-Look Cell 7

    2.2 Single Mover in Multi-Look Cell 8

    2.3 Large Number of Looks 12

3. Gaussian Moving Target Model 19

    3.1 Mover Dimension on the Order of the Multi-Look Cell Size . . 19

    3.2 Mover Dimension on the Order of the Single-Look Cell Size . . 26

4. Measures of Quality 28

    4.1 Probability of Detection for varying SCR 29

    4.2 Receiver Operating Characteristics 31

5. Summary and Conclusions 32

References 34

Annexes 37

A Jacobian 37

B The Noncentral Complex Wishart Distribution 38

C Generalized Bartlett's Theorem for the Noncentral Complex Wishart Distribution 39

C.1 Standard Normal Distribution 39

C.2 Extension to General Case 40

List of figures

1 Joint probability density function of the SAR interferogram including a deterministic target with phase 1.3 rad and SCR of 0 dB. Number of looks $n = 2$. 11

2 Phase probability density function of the SAR interferogram including a deterministic target with phase 1.3 rad and varying SCR. Number of looks $n = 2$. 11

3 Joint probability density function of the SAR interferogram including a deterministic target with phase 1.3 rad and SCR of 0 dB. Number of looks is $n = 3$. 15

4 Joint probability density function of the SAR interferogram including a deterministic target with phase 1.3 rad and SCR of 0 dB. Number of looks $n = 9$. 16

5 Joint probability density function of the SAR interferogram including a deterministic target with phase 1.3 rad and SCR of 20 dB. Number of looks $n = 3$. 16

6 Joint probability density function of the SAR interferogram including a deterministic target with phase 1.3 rad and SCR of 20 dB. Number of looks $n = 6$. 17

7 Phase probability density function of the SAR interferogram including a deterministic target with phase 1.3 rad. Number of looks $n = 3$. 17

8 Phase probability density function of the SAR interferogram including a deterministic target with phase 1.3 rad. Number of looks $n = 6$. 18

9 Joint probability density function of the SAR interferogram including a Gaussian target with phase 1.3 rad and SCR of 0 dB. Number of looks $n = 1$. 21

10 Joint probability density function of the SAR interferogram including a Gaussian target with phase 1.3 rad and SCR of 20 dB. Number of looks $n = 1$. 22

11 Joint probability density function of the SAR interferogram including a Gaussian target with phase 1.3 rad and SCR of 0 dB. Number of looks $n = 3$. 22

12 Joint probability density function of the SAR interferogram including a Gaussian target with phase 1.3 rad and SCR of 20 dB. Number of looks $n = 3$. 23

13 Phase probability density function of the SAR interferogram including a Gaussian target with phase 1.3 rad and varying SCR. Number of looks $n = 1$. 23

14 Phase probability density function of the SAR interferogram including a Gaussian target with phase 1.3 rad and varying SCR. Number of looks $n = 9$. 24

15 Phase probability density function of the SAR interferogram including a Gaussian target with phase 1.3 rad, coherence $\rho_s = 0.99$ and varying SCR. Number of looks $n = 9$. 25

16 Phase probability density function of the SAR interferogram including a Gaussian target with phase 1.3 rad, coherence $\rho_s = 0.91$ and varying SCR. Number of looks $n = 9$. 25

17 Phase probability density function of the SAR interferogram including a Gaussian target in only three one-look cells with phase 1.3 rad and varying SCR. Number of looks $n = 9$. Theoretical curves are calculated with $\beta/3$ and $n = 6$. 27

18 Probability of detection versus SCR for varying number of looks. . . 29

19 Probability of detection versus SCR for varying target Doppler phases (target velocities). 30

20 Probability of detection versus false alarm rate for varying SCR. . . 31

List of tables

1 Phase thresholds for varying number of looks 29

Acknowledgements

The author would like to cordially thank Prof. Alfonso Farina of Alenia Marconi Systems, Rome, Italy for initiating this work and supporting it with fruitful discussions and suggestions.

Furthermore, I thank him and my colleague Ishuwa Sikaneta for the careful proof-reading of the manuscript.

1. Introduction

In air-to-ground radar surveillance it is desirable to be able to detect small moving targets within strong ground clutter. One possible way to achieve this is with Along-Track SAR Interferometry (ATI). ATI exploits the difference in the echoes of two channels observing the same scene at different times. These channels are aligned in the flight direction of the platform. For stationary terrain the two channel signals are identical and can be canceled out (clutter suppression) by computing the phase difference, i.e., the interferogram, leaving only the moving targets in the differential data. Precise knowledge of the interferogram's phase and amplitude statistics is crucial for the development of statistically based detector tests for distinguishing the moving targets from clutter. The statistics of interferograms for different types of stationary clutter have been intensively studied in the past [1, 2, 3, 4].

The multilook phase difference between the two channel outputs z_i is

$$\Psi = \arg\left(\frac{1}{n}\sum_{k=1}^{n} z_1(k) z_2(k)^*\right), \tag{1}$$

where n denotes the number of independent samples, traditionally called number of looks. Under the assumption of Gaussian distributed clutter, the density function was shown to be

$$\begin{aligned} f_\Psi(\psi) = \; & \frac{\Gamma(n+1/2)\left(1-\rho^2\right)^n \rho\cos\psi}{2\sqrt{\pi}\Gamma(n)\left(1-\rho^2\cos^2\psi\right)^{n+1/2}} \\ & + \frac{\left(1-\rho^2\right)^n}{2\pi}\; {}_2F_1(n,1;1/2;\rho^2\cos^2\psi) \end{aligned} \tag{2}$$

for $-\pi < \psi \leq \pi$ [1, 3]. Herein, ${}_2F_1(\cdot)$ denotes the Gauss hypergeometric function, see e g. [5]. The pdf of eq. (2) depends only on the number of looks n and the magnitude of the complex correlation coefficient $\rho\exp(\theta)$.

In the past SAR-ATI has been mainly treated in the context of measurement of sea surface currents [6, 7], though the capability for sensitive ground moving target indication (GMTI) is obvious. Although the effectiveness of ATI for GMTI has been recently evaluated with real data from several experiments [8, 9] no thoroughly theoretic discussion has yet been provided.

The purpose of this technical report is to investigate the probability density function of the SAR interferogram when target signals are superimposed upon the clutter echoes. Depending on the spatial scale of the resolution cell, this density function is used to define detection tests for slowly moving targets. In a previous work [4], only the simplest statistical test case, namely, whether the contents of the image cell in question were target only or clutter only, was considered. The underlying assumption was that the dimension of the moving targets is on the order of the spatial geometric resolution of the SAR and that the backscatter power contained in the cell only resulted from the desired target, i.e., the clutter (or speckle) power was negligible. Therefore, only the density function of the clutter was required to create the test, i.e., to determine a suitable threshold [4].

In cases where the resolution cell size is larger than the target size, the clutter power can no longer be neglected. Here, the hypothesis "clutter only" has to be tested against the alternative "clutter plus target". This general test problem represents the more practical case that a cell contains both clutter and target at the same time. In this context, it is interesting to note that the SAR typical effect of spatial displacement of moving targets within the SAR image substantiates the assumption that a target signal is always contaminated with clutter power. Even with the terrain (clutter) underneath the mover masked out by the vehicle's body, the body is imaged displaced, and hence, superimposed upon clutter at a different "wrong" location. This "wrong clutter" might not even be physically reasonable, e.g., the moving target is imaged on top of a building instead of an adjacent street, which may result in more difficult detection due to a decreased Signal-to-Clutter ratio (SCR).

Depending on the spatial dimension of the moving target compared to the multilook cell size and the type of backscattering model, i.e., deterministic versus random target echo, several models are theoretically investigated in the subsequent chapters. The derived density functions for most models are then graphically illustrated and numerically confirmed with simulated interferometric SAR data. Finally, the performance limits of such detectors are determined via two well known measures of quality, i.e., the probability of detection versus varying SCR on one hand and versus the false alarm rate on the other hand. The latter plot is generally known as the receiver operating characteristics (ROC) of a detector. Both measures depend also on the chosen number of looks and on the resulting interferometric Doppler

phase value, i.e., the radial velocity of the moving target.

1.1 Stationary Clutter Model

Let the zero-mean complex signals of N different channels define the column vector $\underline{Z} = [Z_1, \cdots, Z_N]^T$, where T denotes the transpose operator. Under some reasonable assumptions [4], $\underline{Z}$, with

$$Z_i = \sigma_i X_i \quad \forall \quad i = 1, \cdots, N \qquad \text{and} \quad X_i \sim \mathcal{N}^{\mathbb{C}}(0, 1), \tag{3}$$

can be modeled as a multivariate complex Gaussian random vector with density

$$f_{\underline{Z}}(\underline{z}) = \frac{1}{\pi^N \det(\mathbf{R})} \exp\left(-\underline{z}^H \mathbf{R}^{-1} \underline{z}\right),$$

where $\mathbf{R}$ denotes the covariance matrix.

The following notational convention has been adopted throughout the report: Random variables are capitalized, their realizations are represented by the corresponding lower case letter. Vectors are underlined and matrices are written bold. The superscript H denotes complex conjugate transpose and $\det(\mathbf{R})$ the determinant of $\mathbf{R}$ [10]. In the case of SAR interferometry usually only two channels are involved [11], i.e., the dimension of $\underline{Z}$ is chosen to be $N = 2$ as shall be adopted from here onwards (without loss of generality), i.e.,

$$\mathbf{R} = \mathtt{E}\underline{Z}\underline{Z}^H = \begin{bmatrix} C_{11} & \sqrt{C_{11}C_{22}}e^{j\theta}\rho \\ \sqrt{C_{11}C_{22}}e^{-j\theta}\rho & C_{22} \end{bmatrix}. \tag{4}$$

The off-diagonal elements $R_{12} = R_{21}^* = \mathtt{E}Z_1 Z_2^*$ of the covariance matrix $\mathbf{R}$ describe the complex interferogram. While for across-track interferometry the interferometric phase θ in eq. (4) depends on the illumination geometry and the terrain elevation, for along-track interferometry this value is assumed to be zero ($\theta = 0$), i.e., the clutter is assumed to be stationary. In cases of internal clutter motion, such as sea surface currents, θ is a function of the current velocity.

In order to reduce the speckle, polarimetric and interferometric data are frequently multilook processed. Multilook interferometric processing requires averaging several independent one-look interferograms. In other words several independent one-look sample covariance matrices are averaged. The

n-look sample covariance matrix is given as

$$\hat{\mathbf{R}} = \frac{1}{n}\sum_{k=1}^{n} \underline{z}_k \underline{z}_k^H, \tag{5}$$

where n is the number of looks and $\underline{z}_k$ the k-th one-look or single-look sample (also called snapshots). The random matrix $\mathbf{A} = n\hat{\mathbf{R}}$ with

$$\begin{aligned} \mathbf{A} &= \begin{bmatrix} A_{11} & \Re(A_{12}) + j\Im(A_{12}) \\ \Re(A_{12}) - j\Im(A_{12}) & A_{22} \end{bmatrix} \\ &= \begin{bmatrix} A_{11} & \alpha e^{j\psi} \\ \alpha e^{-j\psi} & A_{22} \end{bmatrix} \end{aligned} \tag{6}$$

is well-known to be complex Wishart-distributed $\mathbf{A} \sim \mathcal{W}_2^{\mathbb{C}}(n, \mathbf{R})$ [10] with probability density

$$f_{\mathbf{A}}(\mathbf{A}) = \frac{\det(\mathbf{A})^{n-2}}{\pi\Gamma(n)\Gamma(n-1)\det(\mathbf{R})^n} \exp\left(-\operatorname{tr}\{\mathbf{R}^{-1}\mathbf{A}\}\right), \tag{7}$$

for $n = 2, 3, 3, \ldots$ Based on this density function, the multilook phase-difference (eq. (2)) and multilook amplitude density functions under the hypothesis "clutter only" have been derived in [1, 2, 3], see also [4].

1.2 Inclusion of Channel Errors and Imbalances

In practice, interference on the returned echo signals from different sources is unavoidable. Such interference could be, for instance, thermal noise in the channels, non-ideal receiver hardware or uncompensated range migration in the SAR processor. The implicit study of the impact on the joint density function of phase and magnitude of the SAR interferogram has been neglected in [1, 2, 3], but has been done for the marginal phase density function (2) in [12]. This subsection describes how to introduce such additional terms into the joint interferogram's probability density function (pdf). As an example additional thermal noise is studied. The general case with arbitrary transfer functions is introduced at the end of the subsection.

In the following, an additional interference $\underline{N} = [N_1, \ldots, N_N]^T$ is modeled as complex normal distributed and stochastically independent between channels as well as independent from the clutter and the moving targets but with different power levels σ_i^2 for $i = 1, \ldots, N$, i.e., $\underline{N} \sim \mathcal{N}_N^{\mathbb{C}}(0, \operatorname{diag}(\sigma_1^2, \ldots,$

$\sigma_N^2)$). Under this assumptions, the covariance matrix in eq. (4) has to be extended to

$$\begin{aligned}\mathbf{K}_N = &\ \mathtt{E}\underline{ZZ}^H + \mathtt{E}\underline{NN}^H \\ = &\ \mathbf{R} + \operatorname{diag}\left(\sigma_1^2, \ldots, \sigma_N^2\right)\end{aligned}$$

which replaces $\mathbf{R}$ in eq. (7) for $N = 2$. Since

$$\begin{aligned}\det\left(\mathbf{K}_N\right) = &\ \left(C_{11} + \sigma_1^2\right)\left(C_{22} + \sigma_2^2\right) - \rho^2 C_{11} C_{22} \\ = &\ C_{11} C_{22}\left(\left(1 + \kappa_1\right)\left(1 + \kappa_2\right) - \rho^2\right), \end{aligned} \tag{8}$$

where $\kappa_1 = \sigma_1^2 / C_{11}$ and $\kappa_2 = \sigma_2^2 / C_{22}$ denote the inverse of the Clutter-to-Noise power Ratio (CNR), and

$$\operatorname{tr}\left(\mathbf{K}_N^{-1}\mathbf{A}\right) = \frac{A_{11}\left(1 + \kappa_2\right)/C_{22} + A_{22}\left(1 + \kappa_1\right)/C_{11} - 2\alpha\rho\sqrt{C_{11}C_{22}}\cos\psi}{C_{11}C_{22}\left[\left(1 + \kappa_1\right)\left(1 + \kappa_2\right) - \rho^2\right]}, \tag{9}$$

the density function of $\mathbf{A}$ becomes

$$\begin{aligned} f(\mathbf{A}) = &\ \frac{\left(A_{11}A_{22} - \alpha^2\right)^{n-2}}{\pi\Gamma(n)\Gamma(n-1)C_{11}^n C_{22}^n\left[\left(1 + \kappa_1\right)\left(1 + \kappa_2\right) - \rho^2\right]^n} \\ &\cdot \exp\left(-\frac{(1 + \kappa_2)A_{11}/C_{11} + (1 + \kappa_1)A_{22}/C_{22} - 2\alpha\rho\cos\psi/\sqrt{C_{11}C_{22}}}{\left(1 + \kappa_1\right)\left(1 + \kappa_2\right) - \rho^2}\right) \\ = &\ \frac{\left(A_{11}A_{22} - \alpha^2\right)^{n-2}}{\pi\Gamma(n)\Gamma(n-1)\overline{C}_{11}^n\overline{C}_{22}^n\left(1 - \overline{\rho}^2\right)^n} \\ &\cdot \exp\left(-\frac{A_{11}/\overline{C}_{11} + A_{22}/\overline{C}_{22} - 2\alpha\overline{\rho}\cos\psi/\sqrt{\overline{C}_{11}\overline{C}_{22}}}{1 - \overline{\rho}^2}\right) \end{aligned} \tag{10}$$

for $A_{11}A_{22} > \alpha^2$. Eq. (10) is identical in form to the stationary clutter in [2], but has modified variances $\overline{C}_{ii} = C_{ii}\left(1 + \kappa_i\right)$ for $i = 1, 2$ and modified coherence

$$\overline{\rho} = \rho / \sqrt{\left(1 + \kappa_1\right)\left(1 + \kappa_2\right)}.$$

Following the derivation in [2], it becomes evident that the joint density function of the interferogram's phase and magnitude remains unchanged in form and that any additional interference only alters (reduces) the coherence between the channels.

Generally, different transfer functions between channels, representing different non-ideal data acquisition hardware and also realistic non-ideal processing system software must be considered. According to the system theoretical

model in [12], the coherence can be written as $\rho = p/\sqrt{q_1 q_2}$ with

$$p = \int H_{11}(\omega) H_{12}(\omega) H_{21}^*(\omega) H_{22}^*(\omega)\ d\omega$$

and

$$q_i = \int |H_{i1}(\omega) H_{i2}(\omega)|^2\ d\omega + \kappa_i \int |H_{i2}(\omega)|^2\ d\omega$$

where $H_{i1}(\omega)$ represents the transfer function of the data acquisition and $H_{i2}(\omega)$ denotes the transfer function of the SAR processor in channel $i \in \{1, 2\}$. Simple analytical models for the different transfer functions can be used to investigate the effect on the coherence and therewith on the density function [12].

2. Deterministic Moving Target Model

As a first intuitive model, a deterministic moving target signal $\underline{s} = \beta[1 \;\; e^{-j\vartheta}]^T$ is considered as superimposed upon the stationary clutter returns in each channel. Without loss of generality, the Doppler phase of targets in the fore channel is set to zero. The real amplitude β determines the signal-to-clutter ratio (SCR). Since n single-look cells of the interferogram are summed, the resulting statistics depend on both the number of moving targets (included in the entire multilook cell) and their dimension compared to the multilook cell size.

2.1 Multiple Movers in Multi-Look Cell

In the most general case, each single-look cell contains a moving point scatterer with different RCS' and different radial velocities. This scenario might happen when observing either urban areas with a potentially large number of movers or extended targets where different scattering centres may have different radial velocity components, such as large ships rolling and pitching in the sea. In such cases, the multilook interferogram is given as

$$I = \frac{1}{n}\sum_{k=1}^{n}(z_1(k) + \beta(k))^* \left(z_2(k) + \beta(k)e^{j\vartheta(k)}\right). \tag{11}$$

Since the targets are assumed deterministic, the model (11) is equivalent to $I = 1/n\sum_{k=1}^{n}\tilde{z}_1(k)^*\tilde{z}_2(k)$ with $\tilde{z}_1(k) = z_1(k) + \beta(k)$ and $\tilde{z}_2(k) = z_2(k) + \beta(k)\exp(j\vartheta(k))$. The composite random vectors $\underline{\tilde{z}}(k) = [\tilde{z}_1(k), \tilde{z}_2(k)]^T$ are mutual independent identical complex normal distributed with expectation $\underline{m}(k) = \beta(k)[1, e^{j\vartheta(k)}]^T$ for $k = 1, \ldots, n$ and covariance matrix $\mathbf{R}$. In contrast to eq. (5), the random matrix

$$\mathbf{A} = n\hat{\mathbf{R}} = \sum_{k=1}^{n}\underline{\tilde{z}}_k\underline{\tilde{z}}_k^H \tag{12}$$

is now noncentral complex Wishart distributed $\mathbf{A} \sim \mathcal{W}_2^{\mathbb{C}}(n, \mathbf{R}, \mathbf{\Omega})$ with noncentrality matrix

$$\mathbf{\Omega} = \mathbf{R}^{-1}\mathbf{M}\mathbf{M}^H, \tag{13}$$

where

$$\mathbf{M} = \begin{bmatrix} \beta(1) & \beta(2) & \cdots & \beta(n) \\ \beta(1)e^{j\vartheta(1)} & \beta(2)e^{j\vartheta(2)} & \cdots & \beta(n)e^{j\vartheta(n)} \end{bmatrix}. \tag{14}$$

Using Annex B, the density function of $\mathbf{A}$ is

$$f(\mathbf{A}) = \frac{\det(\mathbf{A})^{n-2}}{\pi\Gamma(n)\Gamma(n-1)\det(\mathbf{R})^n} e^{-\operatorname{tr}(\mathbf{\Omega})} e^{-\operatorname{tr}\left(\mathbf{R}^{-1}\mathbf{A}\right)} \; {}_0F_1(n; \mathbf{\Omega}\mathbf{R}^{-1}\mathbf{A}),$$

for $\mathbf{A}$ being positive definite, which is in abbreviated form written as $\mathbf{A} > 0$ from here onwards. As this density function contains a hypergeometric function of matrix arguments, analytical analysis is exceedingly complicated. However, for two practical special cases statistical evaluation becomes possible.

2.2 Single Mover in Multi-Look Cell

Regarding high resolution SAR systems with resolutions in the meter-range, the assumption of a single moving target within a multilook cell for a reasonable number of looks ~ 10 seems adequate. This mover can either be a single point scatterer or an extended target consisting of several scattering centres with approximatively the same amplitudes and radial velocities, such as a tank or a large truck etc. The underlying test problem reduces to

$$I = \sum_{k=1}^{n} (z_1(k) + \beta)^* \left(z_2(k) + \beta e^{j\vartheta}\right) \qquad \text{Target phase } \vartheta \text{ known} \quad (15)$$

$$\beta \in \mathbb{R}$$

$$\text{Hypothesis} \qquad H : \beta = 0$$

$$\text{Alternative} \qquad K : \beta > 0.$$

Under the assumption, that the target covers only $q < n$ single look cells, the matrix of expectation vectors in eq. (13) is given as

$$\mathbf{M} = \beta \begin{bmatrix} 1 \\ e^{j\vartheta} \end{bmatrix} \underline{q}^T,$$

where the vector $\underline{q}$ has q components equal to one and the rest zeros, e.g.,

$$\underline{q} = [1, 1, \ldots, 1, 0, \ldots, 0]^T.$$

In this case the matrix product $\mathbf{M}\mathbf{M}^H$ (and therewith also the noncentrality parameter $\mathbf{\Omega} = \mathbf{R}^{-1}\mathbf{M}\mathbf{M}^H$) has rank one. Denoting the signal vector as $\underline{s} = \beta[1, e^{j\vartheta}]^T$, the noncentrality matrix can be written as $\mathbf{\Omega} = q\mathbf{R}^{-1}\underline{s}\underline{s}^H$. Using the annotation in Annex C.2, the density function of $\mathbf{A}$ can be reduced

to involve only hypergeometric functions of scalar arguments. Changing the variable $\mathbf{B}$ in eq. (C.3) to

$$\mathbf{A} = \mathbf{W}^{-1}\mathbf{B}\mathbf{W}^{-H} = \mathbf{R}^{\frac{1}{2}}\mathbf{U}\mathbf{B}\mathbf{U}^{H}\mathbf{R}^{\frac{1}{2}},$$

with Jacobian $J = \det(\mathbf{R})^2$, $\det(\mathbf{B}) = \det(\mathbf{R})^{-1}\det(\mathbf{A})$ and $\operatorname{tr}(\mathbf{B}) = \operatorname{tr}(\mathbf{R}^{-1}\mathbf{A})$ leads to

$$f(\mathbf{A}) = \frac{\det(\mathbf{A})^{n-2}}{\pi\Gamma(n)\Gamma(n-1)\det(\mathbf{R})^{n}} e^{-\operatorname{tr}\left(\mathbf{R}^{-1}\mathbf{A}\right)} e^{-\lambda}\ {}_0F_1(n;\lambda\kappa), \tag{16}$$

where

$$\kappa = \underline{u}_1^{H}\mathbf{R}^{-\frac{1}{2}}\mathbf{A}\mathbf{R}^{-\frac{1}{2}}\underline{u}_1$$

and

$$\lambda = \underline{u}_1^{H}\mathbf{R}^{-\frac{1}{2}}\mathbf{M}\mathbf{M}^{H}\mathbf{R}^{-\frac{1}{2}}\underline{u}_1.$$

Further it is easy to verify that the first eigenvector $\underline{u}_1$ and the only nonzero eigenvalue λ of the matrix

$$\mathbf{R}^{-\frac{1}{2}}\mathbf{M}\mathbf{M}^{H}\mathbf{R}^{-\frac{1}{2}} = q\mathbf{R}^{-\frac{1}{2}}\underline{s}\underline{s}^{H}\mathbf{R}^{-\frac{1}{2}}$$

are

$$\underline{u}_1 = \frac{\mathbf{R}^{-\frac{1}{2}}\underline{s}}{\sqrt{\underline{s}^{H}\mathbf{R}^{-1}\underline{s}}}, \tag{17}$$

and

$$\lambda = q\underline{s}^{H}\mathbf{R}^{-1}\underline{s}. \tag{18}$$

Inserting eqs. (17) and (18) into eq. (16) finally yields the density function of $\mathbf{A}$

$$\begin{aligned} f(\mathbf{A}) = \ & \frac{\det(\mathbf{A})^{n-2}}{\pi\Gamma(n)\Gamma(n-1)\det(\mathbf{R})^{n}}\ \exp\left(-\operatorname{tr}\left\{\mathbf{R}^{-1}\mathbf{A}\right\}\right) \\ & \cdot\exp\left(-q\underline{s}^{H}\mathbf{R}^{-1}\underline{s}\right)\ {}_0F_1(n;q\underline{s}^{H}\mathbf{R}^{-1}\mathbf{A}\mathbf{R}^{-1}\underline{s}). \end{aligned} \tag{19}$$

The equivalent density function for real variables (when the noncentrality matrix has rank one) was originally derived by Anderson and Girshick [13, 14] where they applied the identity

$${}_0F_1(a;X) = \frac{\Gamma(a)}{\sqrt{X}^{a-1}} I_{a-1}\left(2\sqrt{X}\right) \tag{20}$$

for the confluent hypergeometric function [15]. $I_\nu(\cdot)$ denotes the modified Bessel function of order ν. After inserting eqs. (4) and (6) into eq. (19), the argument of the hypergeometric function yields

$$q\underline{s}^H\mathbf{R}^{-1}\mathbf{A}\mathbf{R}^{-1}\underline{s} = q\frac{\beta^2}{1-\rho^2}\left[\left(1+\rho^2-2\rho\cos\vartheta\right)(A_{11}+A_{22}) + 2\alpha\left(\cos(\vartheta+\psi)+\rho^2\cos(\vartheta-\psi)-2\rho\cos\psi\right)\right]. \quad (21)$$

In order to get the interferogram's joint density function of phase and magnitude, eq. (19) has to be integrated with respect to A_{11} and A_{22}. The analytical integration is extremely difficult and leads to awkward terms for the density; therefore, instead, a numerical integration has been performed in Fig. 1 to illustrate the joint density function. The pdf has been computed with the number of looks equal to two and a coherence of $\rho = 0.95$. The target phase is $\vartheta = 1.3$ rad and the SCR has been chosen to 0 dB.

The peak of the pdf is seen to be centered between the target and clutter phases, and possesses nonsymmetric tails in both magnitude and phase. The migration of the density function from the clutter phase at zero towards the target phase for increasing SCR is demonstrated in Fig. 2, where the marginal density function of the phase is plotted. When the SCR tends to infinity, the phase density function becomes a delta-function at the clutter Doppler phase because the random clutter component is negligible.

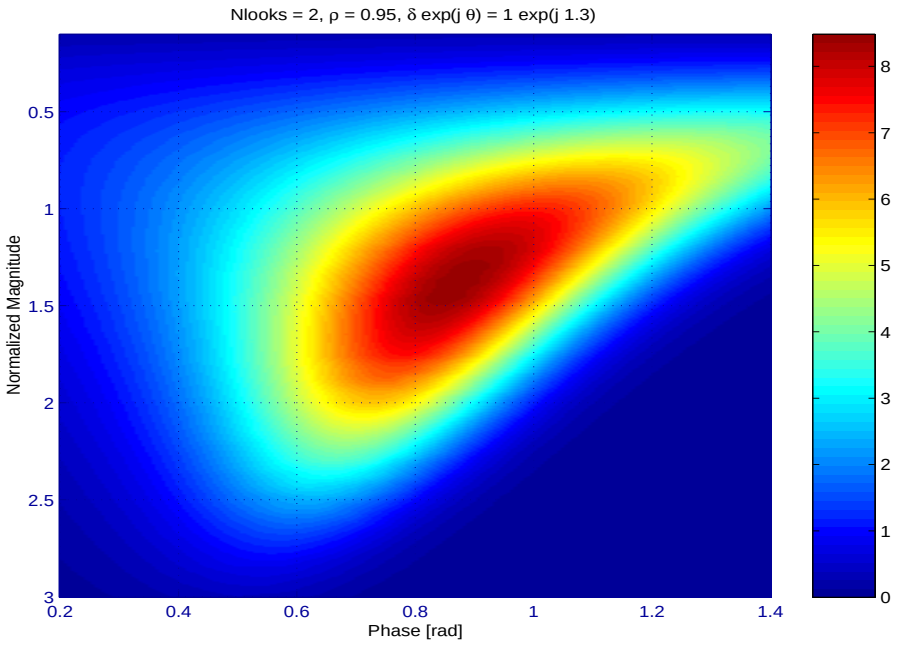

Figure 1 : *Joint probability density function of the SAR interferogram including a deterministic target with phase* 1.3 *rad and SCR of* 0 *dB. Number of looks* $n = 2$.

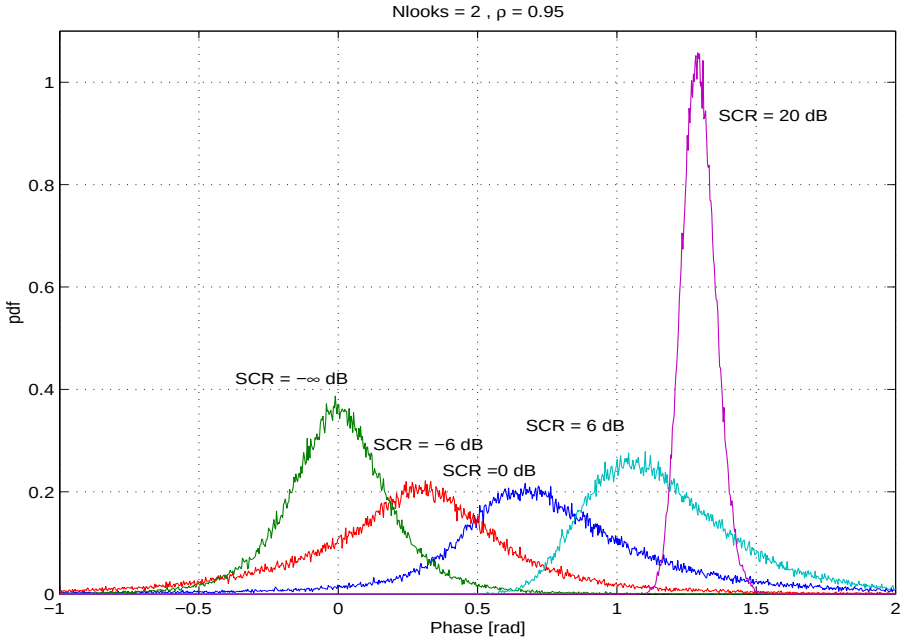

Figure 2 : *Phase probability density function of the SAR interferogram including a deterministic target with phase* 1.3 *rad and varying SCR. Number of looks* $n = 2$.

2.3 Large Number of Looks

A complete analytical description of the joint density function is feasible for the case where the number of looks is large. After multiplying out the terms in eq. (15)

$$I = \frac{1}{n}\sum_{k=1}^{n}\left(z_1(k)^* z_2(k) + \beta^2 e^{j\vartheta}\right) + \frac{1}{n}\sum_{k=1}^{n}\left(z_1(k)^*\beta e^{j\vartheta} + \beta z_2(k)\right),$$

it can be seen that the second sum (of independent random variables with zero mean) tends to zero for increasing n. Hence the test problem can be approximated to a superposition of the target signal on the interferogram rather than on the separate channel outputs:

$$\begin{aligned} I = \frac{1}{n}\sum_{k=1}^{n}\left(z_1(k)^* z_2(k) + \beta e^{j\vartheta}\right) \qquad & \text{Target phase } \vartheta \text{ known} \qquad (22)\\ & \beta \in \mathbb{R} \\ \text{Hypothesis} \qquad & H : \beta = 0 \\ \text{Alternative} \qquad & K : \beta > 0. \end{aligned}$$

For notational convenience, the parameter β^2 describing the amplitude of the target signal has been replaced by β without loss of generality. To calculate the interferogram's statistics under the alternative in eq. (22), the derivation of Lee et. al. [2] for the stationary clutter has to be extended. Let

$$\mathbf{S} = \underline{s}\underline{s}^H = \begin{bmatrix} \beta & \beta e^{j\vartheta} \\ \beta e^{-j\vartheta} & \beta \end{bmatrix}$$

be the deterministic matrix describing the moving target signal, such that

$$\mathbf{B} = \mathbf{A} + \mathbf{S} = n\hat{\mathbf{R}} + \mathbf{S} = \sum_{k=1}^{n} \underline{z}_k \underline{z}_k^H + \mathbf{S}. \qquad (23)$$

The interesting random variables, describing the interferogram of clutter plus target, are again the off-diagonal elements of $\mathbf{B}$. The matrix $\mathbf{B}$ is positive definite for $n \geq 2$. The density function of $\mathbf{B}$ can therefore be calculated as

$$\begin{aligned} f_{\mathbf{B}}(\mathbf{B}) = \; & f_{\mathbf{A}}(\mathbf{B} - \mathbf{S}) \\ = \; & \frac{\det(\mathbf{B} - \mathbf{S})^{n-2}}{\pi\Gamma(n)\,\Gamma(n-1)\det(\mathbf{R})^n} \exp\left(-\operatorname{tr}\{\mathbf{R}^{-1}(\mathbf{B} - \mathbf{S})\}\right). \qquad (24) \end{aligned}$$

Using eq. (6), the determinant in eq. (24) is given as

$$\begin{aligned}\det(\mathbf{B}-\mathbf{S}) = &\ (A_{11}-\beta)(A_{22}-\beta) - \left(\alpha e^{j\psi}-\beta e^{j\vartheta}\right)\left(\alpha e^{-j\psi}-\beta e^{-j\vartheta}\right) \\ = &\ (A_{11}-\beta)(A_{22}-\beta) \\ &-\alpha^2-\beta^2+2\alpha\beta\cos(\psi-\vartheta) > 0. \end{aligned} \tag{25}$$

Using the inverse of the covariance matrix

$$\mathbf{R}^{-1} = \frac{1}{C_{11}C_{22}(1-\rho^2)}\begin{bmatrix} C_{22} & -\rho\sqrt{C_{11}C_{22}} \\ -\rho\sqrt{C_{11}C_{22}} & C_{11}\end{bmatrix},$$

the trace is given as

$$\begin{aligned}\mathrm{tr}\{\mathbf{R}^{-1}(\mathbf{B}-\mathbf{S})\} = &\ \frac{(A_{11}-\beta)/C_{11}+(A_{22}-\beta)/C_{22}}{1-\rho^2} \\ &-\frac{2\rho\alpha/\sqrt{C_{11}C_{22}}\cos(\psi)+2\rho\beta/\sqrt{C_{11}C_{22}}\cos(\vartheta)}{1-\rho^2}. \end{aligned} \tag{26}$$

Changing the random variables from $(A_{11}-\beta)/C_{11}$,$(A_{22}-\beta)/C_{22}$,$\Re(A_{12})$, $\Im(A_{12})$ to $B_1, B_2, \eta = \alpha/\sqrt{C_{11}C_{22}}$ introduces the Jacobian

$$\det(\mathbf{J}) = 1/(C_{11}^2 C_{22}^2 \eta)$$

(see Appendix A). Now, denoting the Signal-to-Clutter ratio (SCR) as $\delta = \beta/\sqrt{C_{11}C_{22}}$ and inserting eq. (25) and eq. (26) into the pdf eq. (24) yields

$$\begin{aligned} f(B_1,B_2,\eta,\psi) = &\ \frac{\left(B_1B_2-\eta^2+2\eta\delta\cos(\psi-\vartheta)-\delta^2\right)^{n-2}}{\pi(1-\rho^2)^n\Gamma(n)\Gamma(n-1)}\eta \\ &\cdot\exp\left(-\frac{B_1+B_2-2\rho\left(\eta\cos(\psi)-\delta\cos(\vartheta)\right)}{1-\rho^2}\right). \end{aligned} \tag{27}$$

Note, that unlike the case with no target, $f(B_1, B_2, \eta, \psi)$ is still a function of C_{11} and C_{22} because of δ. The pdf of magnitude and phase is obtained by integrating eq. (27) over B_1 and B_2. The integration domain is constrained by $B_1B_2 - \eta^2 + 2\eta\delta\cos(\psi-\vartheta) - \delta^2 > 0$ because the matrix $\mathbf{B}$ is positive definite. Integrating first with respect to B_2 and introducing $a = \delta\cos(\psi-\vartheta)$ and $b = \delta\sin(\psi-\vartheta)$ yields

$$\begin{aligned} f(B_1,\eta,\psi) = &\ \frac{\eta B_1^{n-2}\exp\left(-\frac{B_1+2\rho(\eta\cos(\psi)-\delta\cos(\vartheta))}{1-\rho^2}\right)}{\pi(1-\rho^2)^n\Gamma(n)\Gamma(n-1)} \\ &\cdot\int_{\frac{(\eta-a)^2+b^2}{B_1}}^{\infty}\left(B_2-\frac{(\eta-a)^2+b^2}{B_1}\right)^{n-2}\exp\left(-\frac{B_2}{1-\rho^2}\right)dB_2. \end{aligned} \tag{28}$$

Using the integration identity from Gradshteyn and Ryzhik [15] (p. 343, 3.382, 2.) we deduce

$$f(B_1,\eta,\psi) = \frac{\eta B_1^{n-2}}{\pi(1-\rho^2)\Gamma(n)} \exp\left(-\frac{(\eta-a)^2+b^2}{(1-\rho^2)B_1}\right) \cdot \exp\left(-\left(B_1 + 2\rho\left[\eta\cos(\psi) - \delta\cos(\vartheta)\right]\right)/(1-\rho^2)\right). \quad (29)$$

Next, we integrate eq. (29) with respect to B_1

$$f(B_1,\eta,\psi) = \frac{\eta}{\pi(1-\rho^2)\Gamma(n)} \exp\left(-\frac{2\rho\left(\eta\cos(\psi) - \delta\cos(\vartheta)\right)}{1-\rho^2}\right) \cdot \int_0^\infty B_1^{n-2} \exp\left(-\frac{B_1}{1-\rho^2}\right) \exp\left(-\frac{(\eta-a)^2+b^2}{(1-\rho^2)B_1}\right) dB_1. \quad (30)$$

Applying the integration identity from Gradshteyn and Ryzhik [15] (p. 363, 3.471, 9.) gives

$$f(\eta,\psi) = \frac{2\eta\left((\eta-a)^2+b^2\right)^{\frac{n-1}{2}}}{\pi(1-\rho^2)\Gamma(n)} \exp\left(\frac{2\rho\left(\eta\cos(\psi) - \delta\cos(\vartheta)\right)}{1-\rho^2}\right) \cdot K_{n-1}\left(\frac{2\sqrt{(\eta-a)^2+b^2}}{1-\rho^2}\right), \quad (31)$$

where $K_\nu(\cdot)$ denotes the modified Bessel function of order ν. Taking into account that the sample covariance matrix is normalized by the number of looks, i.e.,

$$\mathbf{B} = \frac{1}{n}\mathbf{A} + \mathbf{S}$$

and

$$f_{\mathbf{B}}(\mathbf{B}) = f_{\mathbf{A}}\left(n\mathbf{B} - n\mathbf{S}\right) \cdot n,$$

the bivariate density function is finally given as

$$f(\eta,\psi) = \frac{2n^{n+1}\eta\left((\eta-\delta\cos(\psi-\vartheta))^2 + \delta^2\sin(\psi-\vartheta)^2\right)^{\frac{n-1}{2}}}{\pi(1-\rho^2)\Gamma(n)} \cdot \exp\left(\frac{2n\rho\left(\eta\cos(\psi) - \delta\cos(\vartheta)\right)}{1-\rho^2}\right) \cdot K_{n-1}\left(\frac{2n\sqrt{(\eta-\delta\cos(\psi-\vartheta))^2 + \delta^2\sin(\psi-\vartheta)^2}}{1-\rho^2}\right). \quad (32)$$

The pdf (32) is illustrated in Fig. 3 for a number of looks equal three and a coherence of $\rho = 0.95$. The target phase is $\vartheta = 1.3$ rad and the SCR

has been chosen as 0 dB. The peak of the pdf is centered between the target phase and the clutter phase at zero and shows a large tail along magnitude and phase (compare also Fig. 5). After increasing the number of looks to $n = 9$, the peak of the pdf moves away from the true target phase value but the entire pdf becomes more symmetric, Fig. 4. Similar qualitative behavior can be seen for a larger SCR of 20 dB in Fig. 5 and 6. In order to verify the derivation, the marginal density function of the phase is compared to simulated data for varying SCR, Fig. 7 and 8. The analytical integration of eq. (32) with respect to the magnitude η is extremely difficult or even impossible. Hence numerical integration was used to calculate the theoretical phase pdf. The perfect agreement of theory and simulation is recognized. Again, the phase pdf tends towards a delta function at the true target phase when the SCR approaches infinity.

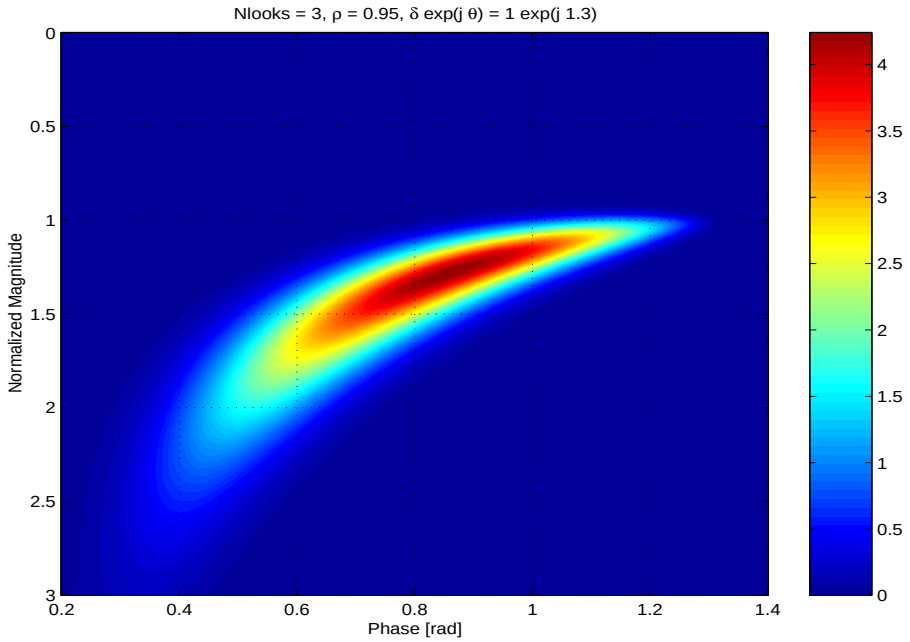

Figure 3 : *Joint probability density function of the SAR interferogram including a deterministic target with phase* 1.3 *rad and SCR of* 0 *dB. Number of looks is* $n = 3$.

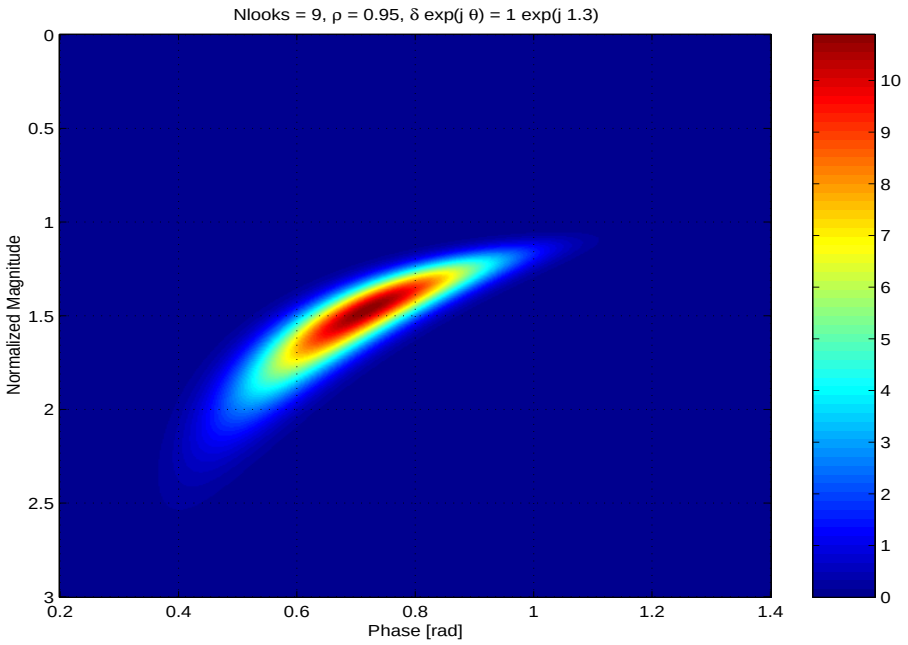

Figure 4 : *Joint probability density function of the SAR interferogram including a deterministic target with phase* 1.3 *rad and SCR of* 0 *dB. Number of looks* $n = 9$.

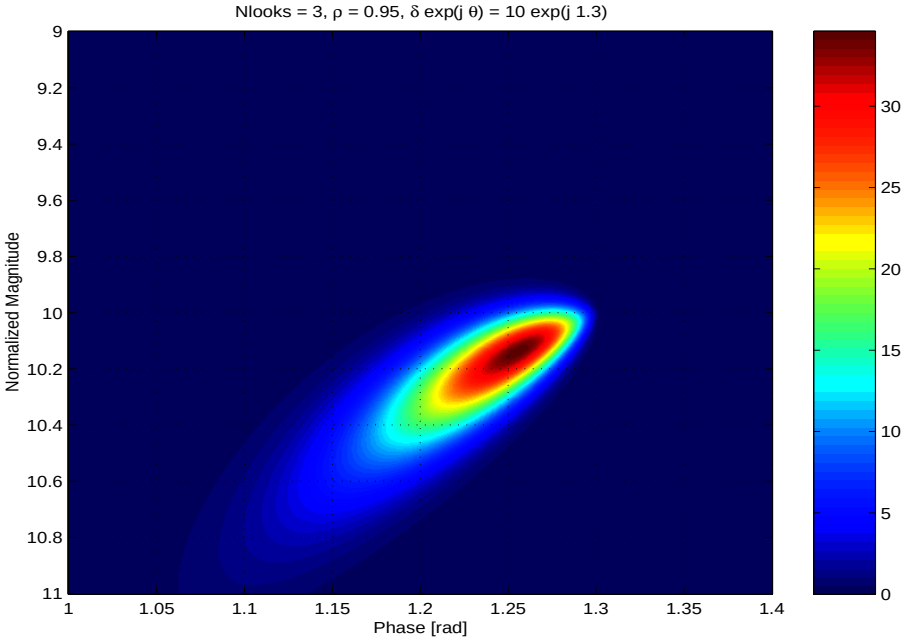

Figure 5 : *Joint probability density function of the SAR interferogram including a deterministic target with phase* 1.3 *rad and SCR of* 20 *dB. Number of looks* $n = 3$.

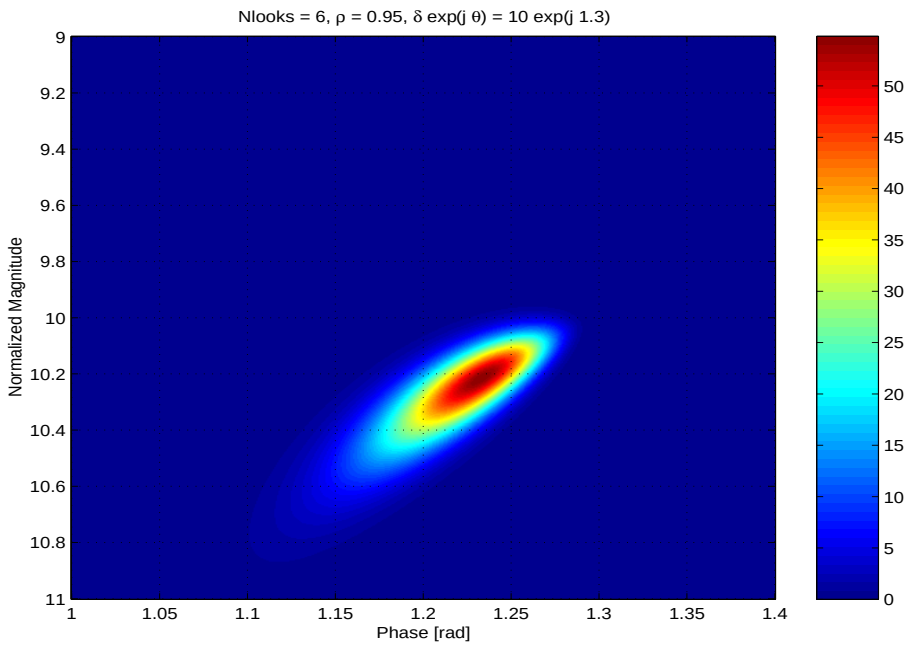

Figure 6 : *Joint probability density function of the SAR interferogram including a deterministic target with phase* 1.3 *rad and SCR of* 20 *dB. Number of looks* $n = 6$.

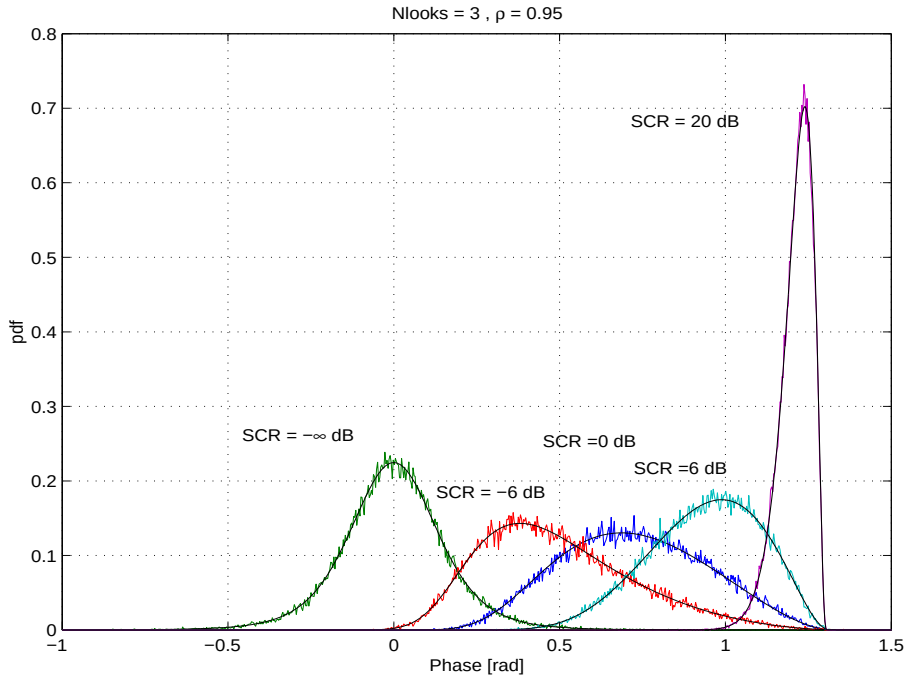

Figure 7 : *Phase probability density function of the SAR interferogram including a deterministic target with phase* 1.3 *rad. Number of looks* $n = 3$.

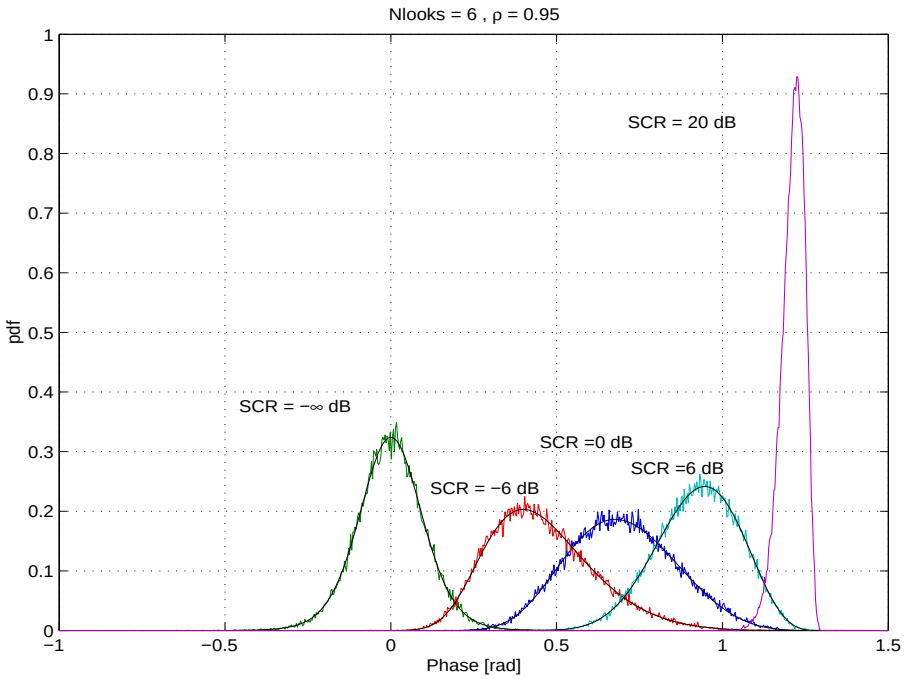

Figure 8 : *Phase probability density function of the SAR interferogram including a deterministic target with phase* 1.3 *rad. Number of looks* $n = 6$.

3. Gaussian Moving Target Model

In the previous test problems it was assumed that the single mover amplitude was constant from one-look cell to one-look cell. In practise this will not be the case because varying propagation conditions, system instabilities, and primarily, variation of the target RCS caused by changing aspect angles are reasons for amplitude fluctuation. If a target consists of many single reflectors, then the backscattered signal is composed of many single contributions with quasi random relative phases. Accordingly, it can be approximated as complex normal distributed. Over short periods of time, e.g., corresponding to the fast-time or range direction in SAR, the aspect angle changes only a little and the amplitude can be assumed to be constant. This model is usually named the Swerling I-case [16]. In the flight direction of the SAR, i.e., slow-time or azimuth direction, the pulses are far enough apart that the amplitudes of the single returns can be considered as stochastically independent. This so-called Swerling II-case is investigated in the subsequent sections. Depending on the geometric resolution compared to the target dimensions two Swerling II applications have to be differentiated.

3.1 Mover Dimension on the Order of the Multi-Look Cell Size

Analogous to the test problem in eq. (11) the alternative, "clutter plus target", can be modeled as

$$I = \frac{1}{n}\sum_{k=1}^{n}\left(Z_1(k) + S_1(k)\right)^* \left(Z_2(k) + S_2(k)\right) \tag{33}$$

where the deterministic target signals have been replaced by the random variables $S_i(k)$ for $i = 1, 2$. As mentioned above, the composite random vector $\underline{S} = [S_1, S_2]^T$ is assumed to be complex normal distributed $\underline{S} \sim \mathcal{N}^{\mathbb{C}}\left(0, \mathbf{K}_S\right)$ with expectation zero and covariance matrix

$$\mathbf{K}_S = \beta \begin{bmatrix} 1 & \rho_s e^{j\vartheta} \\ \rho_s e^{-j\vartheta} & 1 \end{bmatrix},$$

where ρ_s denotes the coherence of the moving target signals. It is important to note that, in the absence of temporal decorrelation, the coherence

between the two channel outputs will be exactly identical for the target and the clutter. However, even with temporal decorrelation, the target coherence can either be larger or smaller than the surrounding clutter coherence. A perfectly steady vehicle, for instance, smoothly moving over a terrain of vegetation might have a larger coherence than the vegetation. The contrary, where the vehicle is rolling and bouncing over terrain which is otherwise perfectly stationary leads to a lower coherence for the target compared to the surrounding terrain.

Since the clutter and the target are mutually stochastically independent, the sum of them will still be complex normal distributed. The resulting sample covariance matrix

$$\begin{aligned}\mathbf{A} = n\hat{\mathbf{R}} = & \sum_{k=1}^{n} (\underline{z}_k + \underline{s}_k)\,(\underline{z}_k + \underline{s}_k)^H \\ = & \sum_{k=1}^{n} \underline{v}_k \underline{v}_k^H, \end{aligned} \tag{34}$$

with $\underline{v}_k = \underline{z}_k + \underline{s}_k$ is therefore complex Wishart distributed $\mathbf{A} \sim \mathcal{W}_m^{\mathbb{C}}\,(n, \mathbf{R} + \mathbf{K}_S)$ with n degrees of freedom. The composite covariance matrix is given as

$$\mathbf{K}_S + \mathbf{R} = \begin{bmatrix} 1+\beta & \rho + \beta\rho_s e^{j\vartheta} \\ \rho + \beta\rho_s e^{-j\vartheta} & 1+\beta \end{bmatrix} = (1+\beta)$$

$$\cdot \begin{bmatrix} 1 & \frac{\sqrt{\rho^2+\beta^2\rho_s^2+2\beta\rho\rho_s\cos\vartheta}}{1+\beta} e^{\mathrm{jatan}\left(\frac{\beta\rho_s\sin\vartheta}{\rho+\beta\rho_s\cos\vartheta}\right)} \\ \frac{\sqrt{\rho^2+\beta^2\rho_s^2+2\beta\rho\rho_s\cos\vartheta}}{1+\beta} e^{-\mathrm{jatan}\left(\frac{\beta\rho_s\sin\vartheta}{\rho+\beta\rho_s\cos\vartheta}\right)} & 1 \end{bmatrix}$$

which has the same form as eq. (4). Hence, the joint density function of the phase and magnitude

$$f_{\mathcal{E},\Psi}(\eta,\psi) = \frac{2n^{n+1}\eta^n}{\pi\Gamma(n)\,(1-\bar{\rho}^2)} \exp\left(\frac{2n\eta\bar{\rho}\cos(\psi-\psi_0)}{1-\bar{\rho}^2}\right) K_{n-1}\left(\frac{2n\eta}{1-\bar{\rho}^2}\right) \tag{35}$$

where K_n is the modified Bessel function of order n [3, 1, 17] remains unchanged compared to the stationary clutter case, except that the coherence ρ and the phase ψ are replaced by

$$\bar{\rho} = \frac{\sqrt{\rho^2 + \beta^2\rho_s^2 + 2\beta\rho\rho_s\cos\vartheta}}{1+\beta} \tag{36}$$

and

$$\psi - \psi_0 = \psi - \arctan\left(\frac{\beta\rho_s \sin\vartheta}{\rho + \beta\rho_s \cos\vartheta}\right). \tag{37}$$

The corresponding marginal phase density function is given in eq. (2).

The coherence of the target and the clutter are the same in the following numerical examples; The effect of different values is investigated later. For increasing SCR values, the phase density becomes wider than the original clutter pdf because the factor $\sqrt{1+\beta^2+2\beta\cos\vartheta}/(1+\beta)$ is always less than one if $\vartheta \neq 0$, assuming that $\rho_s = \rho$.

At the same time the peak of the pdf migrates towards the target phase value ϑ. When the SCR tends to infinity ($\beta \to \infty$), $\bar{\rho}$ tends to ρ and ψ_0 towards ϑ, i.e., the phase density function in that case is identical to the original clutter pdf except for the Doppler shift towards the target frequency. This behavior of the joint density function is illustrated in Figs. 9-12 for different SCR's and number of looks n, and for the marginal phase densities in Figs. 13-14. The perfect agreement of theory and simulation can be recognized again.

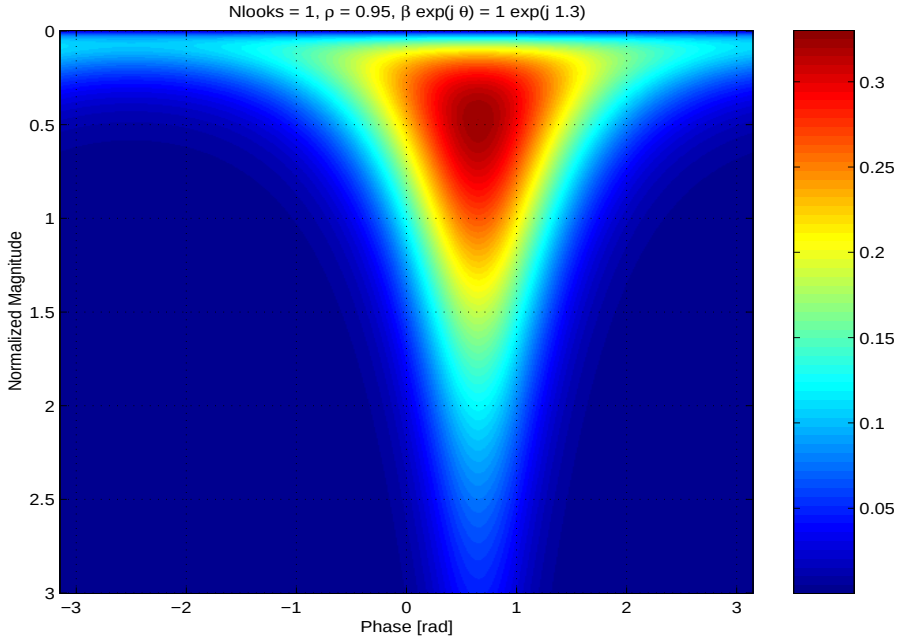

Figure 9 : *Joint probability density function of the SAR interferogram including a Gaussian target with phase* 1.3 *rad and SCR of* 0 *dB. Number of looks* $n = 1$.

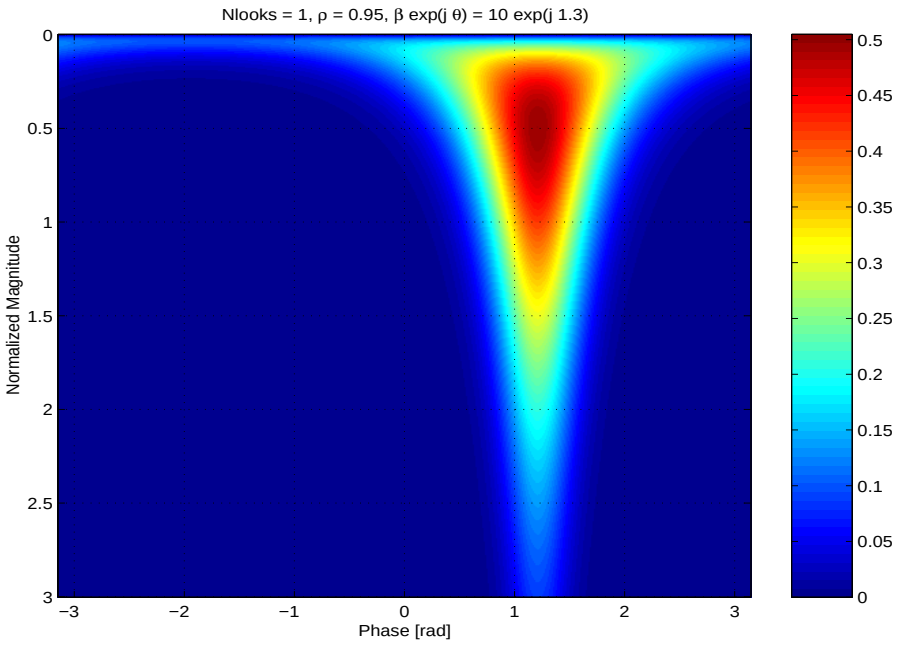

Figure 10 : *Joint probability density function of the SAR interferogram including a Gaussian target with phase* 1.3 *rad and SCR of* 20 *dB. Number of looks* $n = 1$.

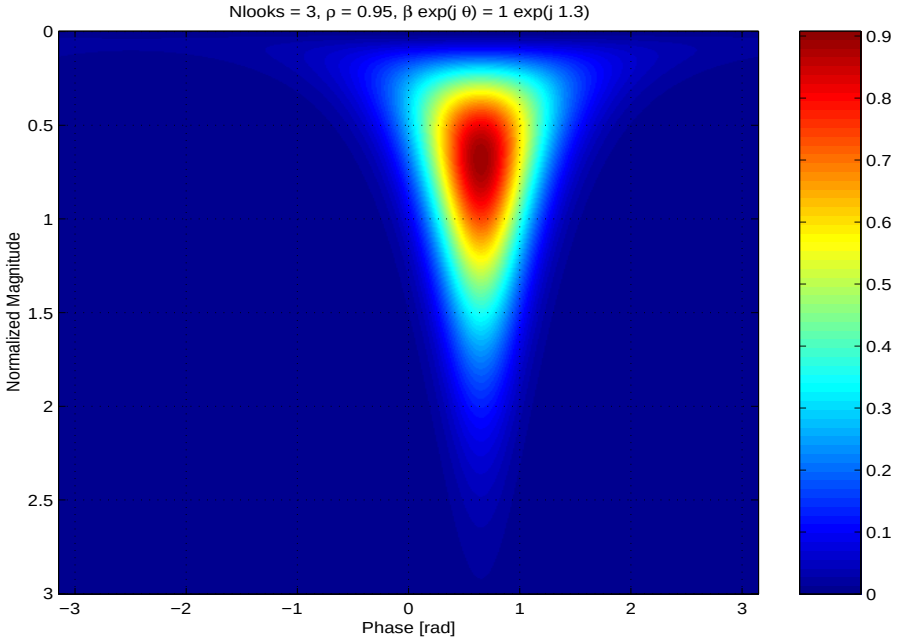

Figure 11 : *Joint probability density function of the SAR interferogram including a Gaussian target with phase* 1.3 *rad and SCR of* 0 *dB. Number of looks* $n = 3$.

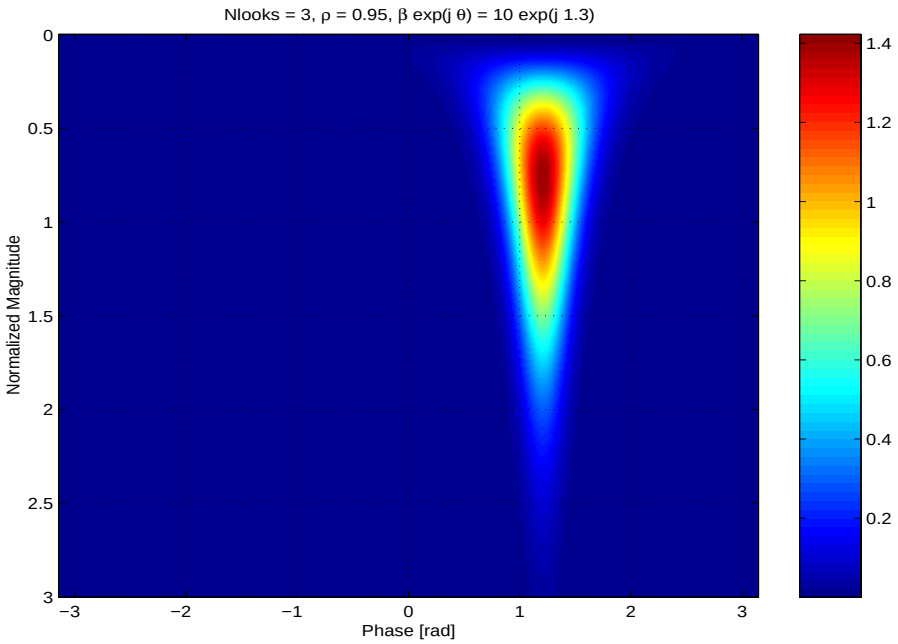

Figure 12 : *Joint probability density function of the SAR interferogram including a Gaussian target with phase* 1.3 *rad and SCR of* 20 *dB. Number of looks* $n = 3$.

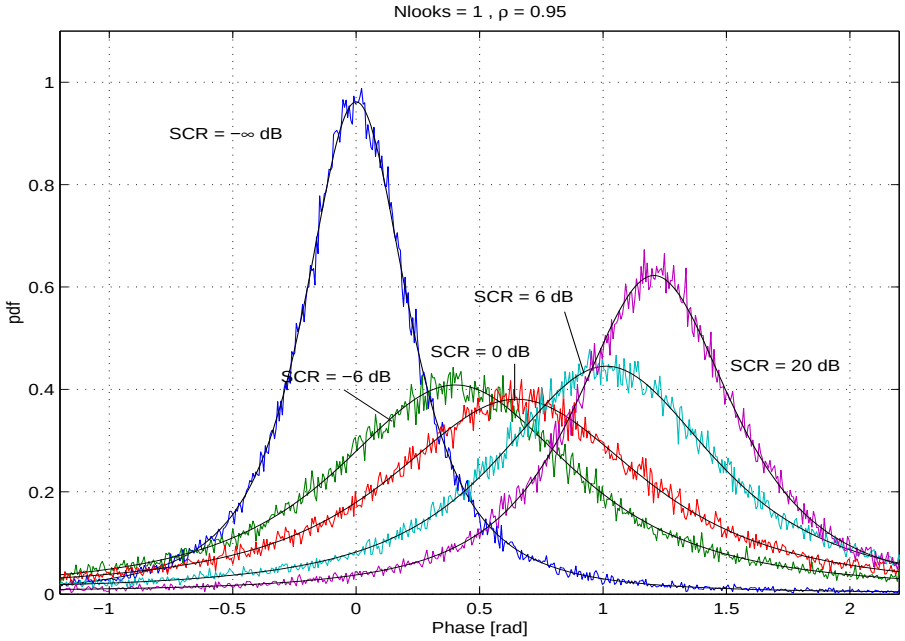

Figure 13 : *Phase probability density function of the SAR interferogram including a Gaussian target with phase* 1.3 *rad and varying SCR. Number of looks* $n = 1$.

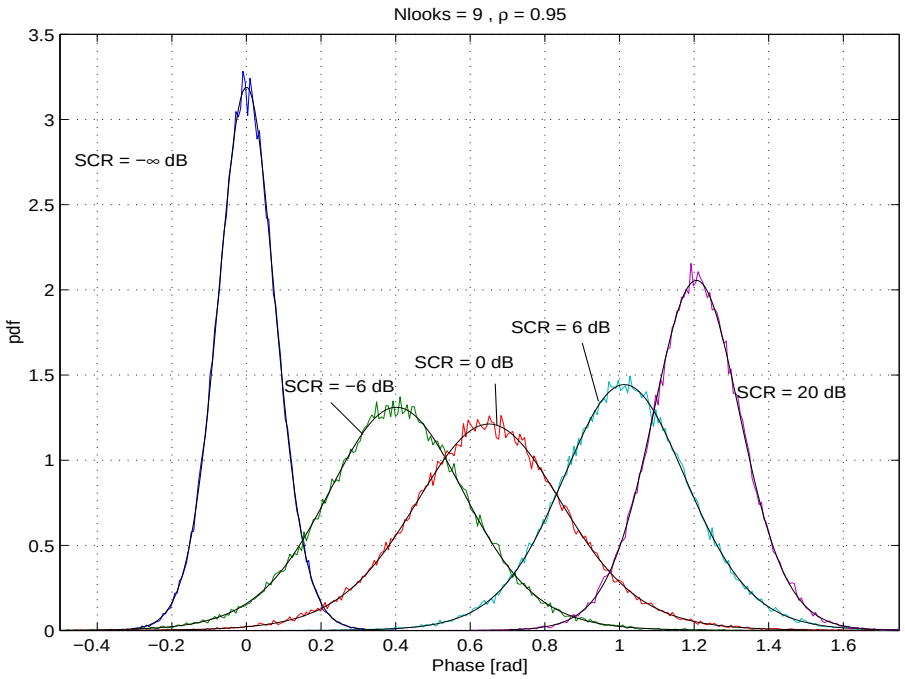

Figure 14 : *Phase probability density function of the SAR interferogram including a Gaussian target with phase* 1.3 *rad and varying SCR. Number of looks* $n = 9$.

In order to study the effects of different correlation values for the target and the clutter, two simulation have been carried out. Figure 15 demonstrates the case of larger coherence of the moving target with $\rho_s = 0.99$ compared to $\rho = 0.95$ for the surrounding clutter. The solid curves represent the density functions for the case that both target and clutter possess identical correlation $\rho = \rho_s = 0.95$. One can see that the mismatch becomes more pronounced for targets with larger SCR, i.e., the resulting density functions are narrower compared to the case of identical coherence. When the correlation of the moving target decreases relative to that of the clutter, Fig. 16, the opposite effect occurs; The density functions widen for larger SCR compared to the identical coherence case. However, both figures also indicate that the overall impact of different correlation values is not expected to be drastical in practice, particularly because the values are not assumed to vary too much within the aperture time (i.e., the time for the aft channel to travel to the previous position of the fore channel). On the contrary, the coherence values are expected to be close in most practical cases.

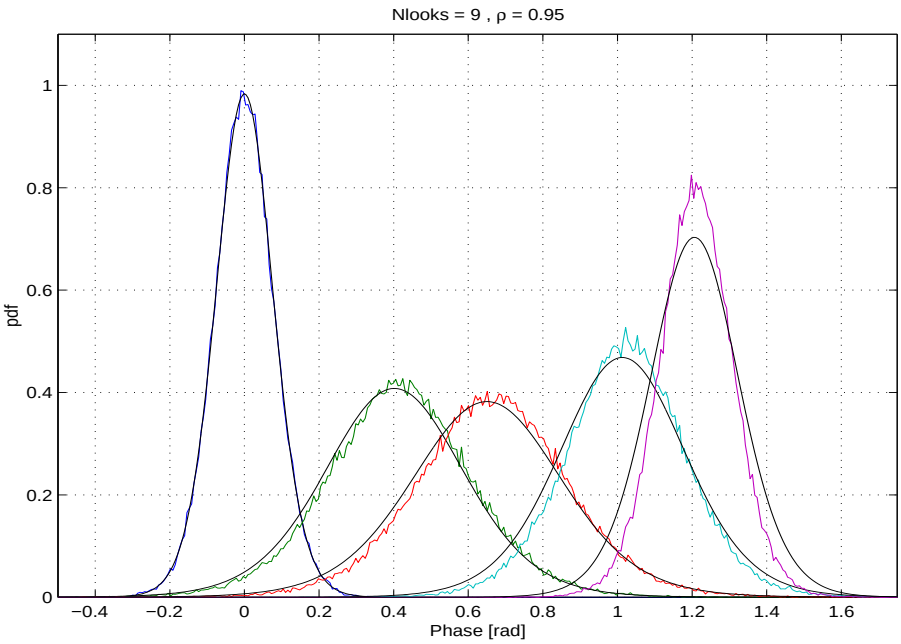

Figure 15 : *Phase probability density function of the SAR interferogram including a Gaussian target with phase* 1.3 *rad, coherence* $\rho_s = 0.99$ *and varying SCR. Number of looks* $n = 9$.

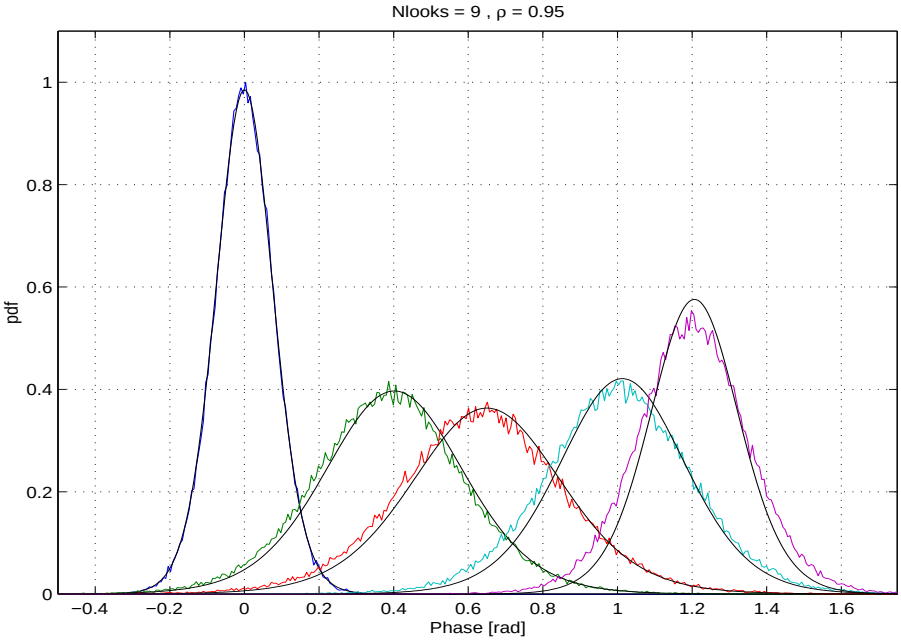

Figure 16 : *Phase probability density function of the SAR interferogram including a Gaussian target with phase* 1.3 *rad, coherence* $\rho_s = 0.91$ *and varying SCR. Number of looks* $n = 9$.

3.2 Mover Dimension on the Order of the Single-Look Cell Size

In cases where the moving target dimension is smaller than the multilook cell size, the model in eq. (33) is no longer adequate. Instead, we get for the sample covariance matrix

$$\begin{aligned}\mathbf{A} &= \sum_{k=1}^{l} (\underline{z}_k + \underline{s}_k)(\underline{z}_k + \underline{s}_k)^H + \sum_{k=l+1}^{n} \underline{z}_k \underline{z}_k^H \\ &= \mathbf{B} + \mathbf{C} \qquad \text{for} \quad l \in \{2, \ldots, n\},\end{aligned}$$

when it is assumed that the mover is only contained in the first l one-look cells. Therefore, the random matrix $\mathbf{A}$ consists of a sum of two independent complex Wishart distributed matrices $\mathbf{B} \sim \mathcal{W}_m^{\mathbb{C}}(l, \mathbf{R} + \mathbf{K}_S)$ and $\mathbf{C} \sim \mathcal{W}_m^{\mathbb{C}}(n-l, \mathbf{R})$. Assuming that there exist density functions for $\mathbf{B}$ and $\mathbf{C}$, i.e., $3 < l < n-1$, the density function of $\mathbf{A}$ is given as the integral

$$\begin{aligned} f(\mathbf{A}) &= \int_{\mathbf{B}>0, \mathbf{A}-\mathbf{B}>0} f_{\mathbf{B}}(\mathbf{B}) f_{\mathbf{C}}(\mathbf{A}-\mathbf{B})\, d\mathbf{B} \qquad (38) \\ &= \frac{\det(\mathbf{R})^{-(n-l+1)} \det(\mathbf{R}+\mathbf{K}_S)^{-(l-1)}}{\pi^2 \Gamma(n-l+1)\Gamma(n-l)\Gamma(l-1)\Gamma(l-2)} \exp\left(-\operatorname{tr}\left((\mathbf{R}+\mathbf{K}_S)^{-1}\mathbf{A}\right)\right) \\ &\quad \cdot \int_{\mathbf{B}>0, \mathbf{A}-\mathbf{B}>0} \det(\mathbf{B})^{n-l-1} \det(\mathbf{A}-\mathbf{B})^{l-3}\, e^{-\operatorname{tr}\left(\left(\mathbf{R}^{-1}-(\mathbf{R}+\mathbf{K}_S)^{-1}\right)\mathbf{B}\right)}\, d\mathbf{B}. \end{aligned}$$

To the best knowledge of the author, such a density function has not yet been derived in closed form.

However, to investigate the difference between the phase densities in section 3.1 and 3.2, a numerical study has been performed. Figure 17 shows the resulting phase histograms when only the three first one-look cells contain the moving target. Other than that, all other parameters are chosen identical to those used in Fig. 14. Two differences can be recognized: on one hand the effective SCR is only a third of the original SCR $\beta/3$ (because the target covers only a three single-look cells out of nine), and on the other hand an increase in variance. The resulting widening of the density functions can be approximatively represented by a loss in the effective number of looks. In Fig. 17, for instance, an effective number of looks of $n = 6$ is assumed for the superimposed theoretical density functions. While this loss can partly be compensated by choosing a larger number of looks for the processing,

the reduction in SCR is inherent and will of course reduce the probability of detection, compare also section 4.

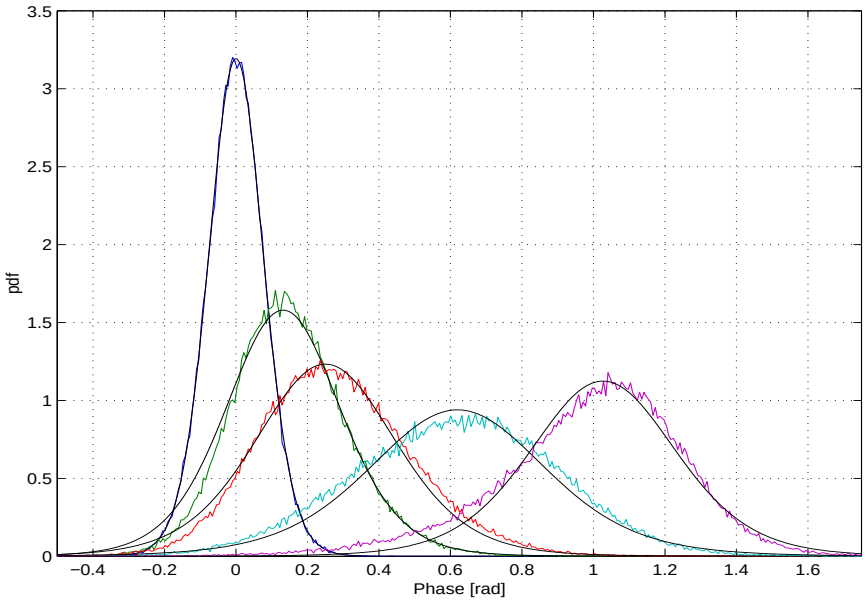

Figure 17 : *Phase probability density function of the SAR interferogram including a Gaussian target in only three one-look cells with phase* 1.3 *rad and varying SCR. Number of looks* $n = 9$*. Theoretical curves are calculated with* $\beta/3$ *and* $n = 6$*.*

4. Measures of Quality

In order to study and compare the performance of the different models for the detectors, two well known measures of quality, i.e., the probability of detection P_d versus SCR, and P_d versus the false alarm rate are studied. As a worst case scenario, only the results for the Gaussian random model are exemplarily introduced, but they could easily be computed for the deterministic target model as well. The coherence of the target and clutter are assumed to be identical.

The probability of detection is defined as

$$\begin{aligned} P_d(\xi) = & \int_{\xi}^{\pi} f_{\Psi}(\psi;\beta,\vartheta)\ d\psi \\ = & \int_{\xi}^{\pi} \frac{\Gamma(n+1/2)\left(1-\bar{\rho}^2\right)^n \bar{\rho}\cos(\psi-\psi_0)}{2\sqrt{(}\pi)\Gamma(n)\left(1-\bar{\rho}^2\cos^2(\psi-\psi_0)\right)^{n+1/2}} \\ & + \frac{\left(1-\bar{\rho}^2\right)^n}{2\pi}\ {}_2F_1(n,1;1/2;\bar{\rho}^2\cos^2(\psi-\psi_0))\ d\psi \end{aligned} \tag{39}$$

where

$$\bar{\rho} = \rho\sqrt{1+\beta^2+2\beta\cos\vartheta}/(1+\beta)$$

and

$$\psi_0 = \arctan(\beta\sin\vartheta/(1+\beta\cos\vartheta)).$$

The threshold ξ must be determined in such a way that the probability of false alarm (or false alarm rate)

$$\begin{aligned} P_f(\xi) = & \int_{\xi}^{\pi} f_{\Psi}(\psi;0,0)\ d\psi \\ = & \int_{\xi}^{\pi} \frac{\Gamma(n+1/2)\left(1-\rho^2\right)^n \rho\cos\psi}{2\sqrt{(}\pi)\Gamma(n)\left(1-\rho^2\cos^2\psi\right)^{n+1/2}} \\ & + \frac{\left(1-\rho^2\right)^n}{2\pi}\ {}_2F_1(n,1;1/2;\rho^2\cos^2\psi)\ d\psi \quad \leq \varepsilon \end{aligned} \tag{40}$$

is always less or equal than a given level ε, i.e., $\xi = F_{\Psi}^{-1}(1-\varepsilon)$, where $F_{\Psi}(\cdot)$ denotes the probability distribution function of Ψ. In the following the integrals in eq. (39) and eq. (40) are numerically evaluated for different sets of target parameters.

4.1 Probability of Detection for varying SCR

In Figure 18 the dependence of the probability of detection P_d on the SCR and the chosen number of looks is investigated. The coherence is $\rho = 0.95$ and the target Doppler phase is held constant at 74° (1.3 rad). It can be recognized that moving targets cannot be detected even for very large SCR when the number of looks is small $n < 4$. The reason for this deficiency is the relatively broad phase distribution for small number of looks so that the threshold (according to the chosen value $\varepsilon = 1e^{-4}$) becomes too large, especially larger than $\vartheta = 1.3$ rad (see Table 1). On the other hand, for

n	1	2	3	4	5	6	7	8	9	10
$\eta_\psi[rad]$	3.123	2.840	1.450	0.846	0.664	0.548	0.448	0.413	0.379	0.341

Table 1: *Phase thresholds for varying number of looks*

larger values of n ($n > 7$) only a small additional gain in performance can be achieved.

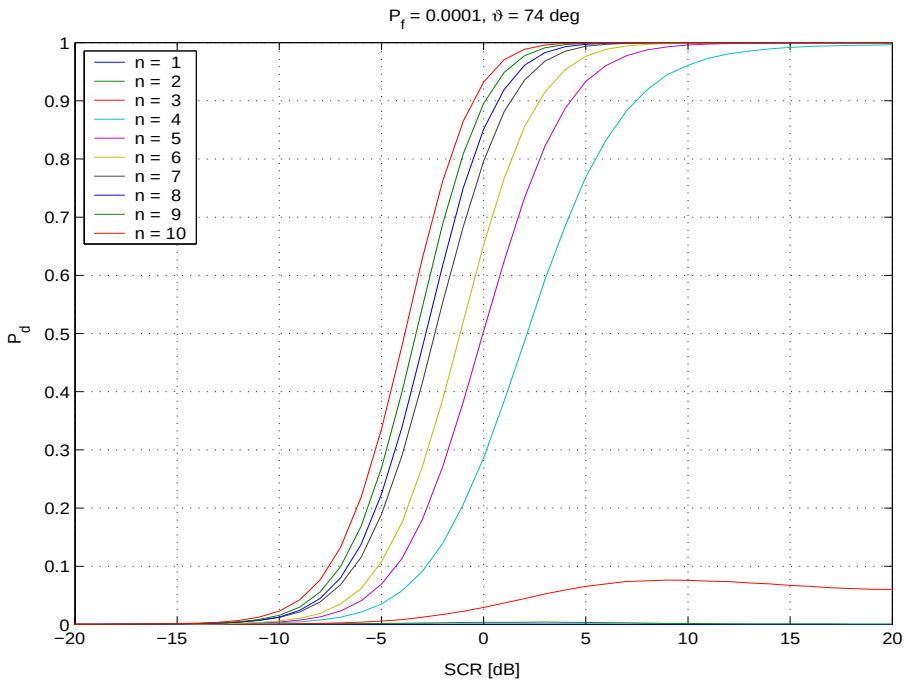

Figure 18 : *Probability of detection versus SCR for varying number of looks.*

In Fig. 19 it is seen that by holding the number of looks constant at $n = 9$, and varying the Doppler phase ϑ from zero to 90° a minimum target

radial velocity corresponding to about $\vartheta = 40°$ is necessary in order to be able to detect the targets for reasonable SCR. According to Table 1, the phase threshold was set to $\eta_\psi = 0.379$ for $n = 9$. Again, after exceeding a certain target velocity, no significant additional gain in detection probability is achieved. Assuming that the two receiving antennas are separated in azimuth by the distance d, the interferometric phase can be a approximated by [18]

$$\Delta\phi = \frac{2\pi}{\lambda} d \frac{v_r}{v_a} \qquad \text{or} \qquad v_r = \Delta\phi \frac{\lambda}{2\pi} \frac{v_a}{d},$$

where λ represents the wavelength, v_r the radial velocity of the target and v_a the velocity of the antenna. Inserting for example, typical space-borne parameters: $\lambda = 5.6$ cm, $v_a \cong 7.5$ km/s and $d = 7.5$ m, yields for $\Delta\phi_{\min} = 40°$ a corresponding minimum target velocity of $v_{r,\min} \cong 6.3$ m/s given a SCR of 5 dB.

Inserting, for instance, some realistic airborne parameters for along-track interferometry, such as $v_a = 100$ m/s and $d = 0.5$ m, yields an even more sensitive system with $v_{r,\min} = 1.23$ m/s.

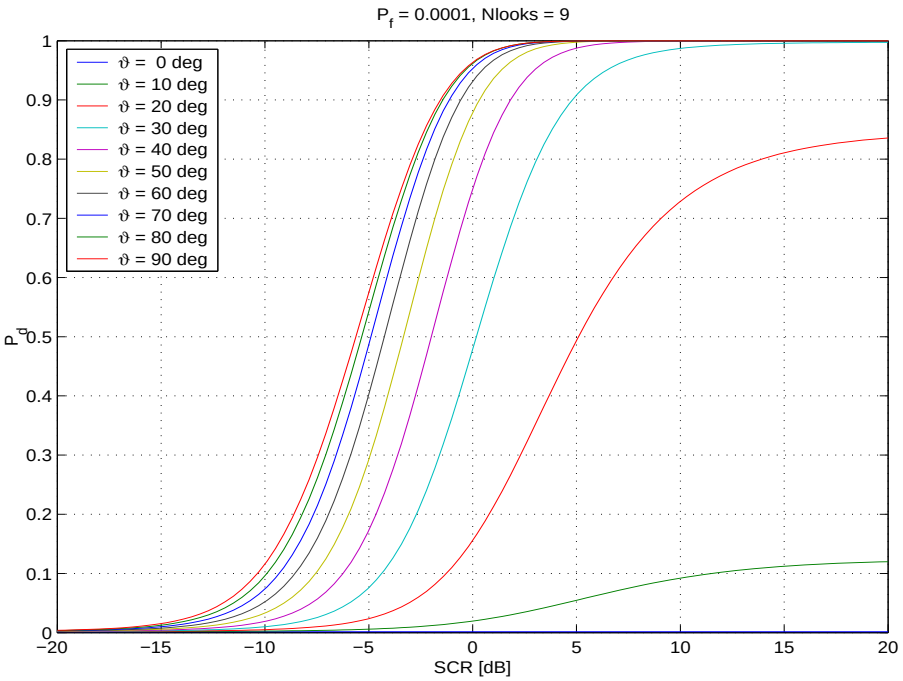

Figure 19 : *Probability of detection versus SCR for varying target Doppler phases (target velocities).*

4.2 Receiver Operating Characteristics

The other important measure of quality is the receiver operating characteristic (ROC), i.e., P_d as a function of P_f for fixed SCR. In Fig. 20 the ROC is shown for the considered test. The number of looks was chosen as $n = 5$ and the target Doppler phase as $\vartheta = 1.3$ rad. For vanishing SCR, $P_d = P_f$ holds; the corresponding curve is the diagonal through the ROC-diagram. For increasing SCR the curves bend upwards under retention of the points $(0, 0)$ and $(1, 1)$. A best test for the alternative is characterized in such a way that no other test exists whose ROC exceeds that of the best test at any position. The ROC provides insight into the minimum allowable P_f for a certain SCR without loosing too many true targets.

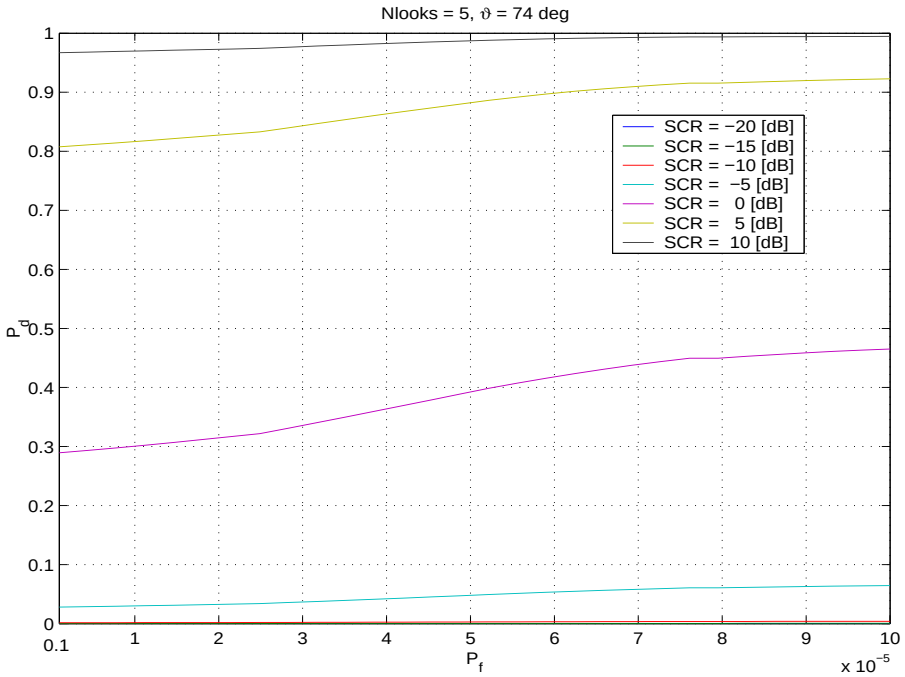

Figure 20 : *Probability of detection versus false alarm rate for varying SCR.*

5. Summary and Conclusions

In this report, the marginal probability density function of the SAR interferogram's phase has been derived analytically in the case where moving target signals are superimposed upon the stationary clutter. Based on the spatial dimension of the moving targets compared to the multi-look cell size, several models, including deterministic as well as Gaussian distributed target returns have been investigated. This theoretical analysis is an extension of the known statistics for the clutter-only case. Most theoretical results were demonstrated and confirmed with simulated interferometric phase data.

All considered models have in common that the peaks of their corresponding phase density functions migrate from zero (stationary clutter) towards the target Doppler phase (introduced by its radial velocity) for increasing SCR. One major difference between the deterministic and random model is that the density of the first tends towards a delta function when the SCR $\rightarrow \infty$, whereas the pdf of the latter preserves a certain width (variance).

In order to study and compare the performance of the different models in more detail, two well known measures of quality, i.e., the probability of detection P_d versus varying SCR and P_d versus the false alarm rate (receiver operating characteristics) were studied based on the derived density functions. These measures provide insight into expected capabilities from upcoming SAR/GMTI systems particularly Radarsat2 and the enhanced airborne Aurora CP-140 SpotSAR system.

One main conclusion of this report is that there exists a quasi-optimum value for the number of independent looks. A good choice for the number of looks for the interferometric processor is in the order of $n = 9$. Smaller numbers than $n = 4$ prohibit almost any detection, larger numbers do not imply any significant gain. In contrast, increasing the number of looks unnecessarily, leads to a loss in geometric resolution.

A reasonable choice for the false alarm rate could be $P_f = 1e^{-4}$, because it would correspond to a single false alarm per 100×100 SAR interferogram pixels. For a SAR system with geometric resolution in meter range, this would roughly lead to one false alarm in an one square-kilometer (1km^2).

For such parameter adjustments one would expect that a space-borne sys-

tem may be able (greater than 98 % chance) to detect targets that have a SCR of > 5 dB when moving faster than approximatively 20 km/h. An airborne SAR system would be about five times more sensitive, i.e., the minimum radial velocity of the moving targets would be in the range of 4 km/h for the same system parameters. Higher velocities or larger SCR, of course, improve the probability of detection.

References

1. Lee, J.-S., Hoppel, K. W., Mango, S. A. and Miller, A. R. (1994). Intensity and Phase Statistics of Multilook Polarimetric and Interferometric SAR Imagery. *IEEE Trans. Geoscience and Remote Sensing*, **GRS-32**(5), 1017–1028.

2. Lee, J.-S., Miller, A. R. and Hoppel, K. W. (1994). Statistics of Phase Difference and Product Magnitude of Multi-Look Processed Gaussian Signals. *Waves in Random Media*, **4**, 307–319.

3. Joughin, I. R., Winebrenner, D. P. and Percival, D. B. (1994). Probability Density Functions for Multilook Polarimetric Signatures. *IEEE Trans. Geoscience and Remote Sensing*, **GRS-32**(3), 562–574.

4. Gierull, C.H. (July 2001). Statistics of SAR Interferograms with Application to Moving Target Detection. Defence Research Establishment Ottawa. (Technical Report TR 2001-045). Canada.

5. Abramowitz, M. and Stegun, I. A. (1970). Handbook of Mathematical Functions, 9 ed. Dover Publications, Inc.

6. Goldstein, R. M. and Zebker, H. A. (1987). Interferometric Radar Measurments of Ocean Surface Currents. *Nature*, **328**(20), 707–709.

7. Bao, M., Brüning, C. and Alpers, W. (1997). Simulation of Ocean Waves Imaging by an Along-Track Interferomtric Synthetic Aperture Radar. *IEEE Trans. Geoscience and Remote Sensing*, **GRS-35**(3), 618–649.

8. Coe, D. and White, D. R. (1995). Moving Target Detection in SAR Imagery: Experimental Results. In *Proc. IEEE Int. Radar Conf.*, pp. 664–669.

9. Livingstone, C., Sikaneta, I., Gierull, C.H., Chiu, S., Beaudoin, A., Campbell, J., Beaudoin, J., Gong, S. and Knight, T. (2002). An Airborne SAR Experiment to Support RADARSAT-2 GMTI. *accepted by Canadian Journal of Remote Sensing*.

10. Goodman, J. W. (1963). Statistical Analysis Based on a Certain Multivariate Complex Gaussian Distribution (An Introduction). *Ann. Math. Stat.*, **34**(152), 152–180.

11. Rodriguez, E and Martin, J. M. (1992). Theory and Design of Interferometric Synthetic Aperture Radars. *IEE Proc.-Radar, Sonar Navig. (Pt. F)*, **139**(2), 147–159.

12. Just, D. and Bamler, R. (1994). Phase Statistics of Interferograms with Applications to Synthetic Aperture Radar. *Applied Optics*, **33**(20), 4361–4367.

13. Anderson, T. W. and Girshick, M. A. (1944). Some Extensions of the Wishart Distribution. *Annals of Mathematical Statistics*, **15**(4), 345–357.

14. Anderson, T. W. (1946). The Non-Central Wishart Distribution and Certain Problems of Multivariate Statistics. *Annals of Mathematical Statistics*, **17**(4), 409–431.

15. Gradshteyn, I. S. and Ryzhik, I. M. (2000). Table of Integrals, Series and Products (Sixth Edition), 6 ed. Academic Press.

16. Skolnik, M. I. (1970). Radar Handbook, New York: McGraw-Hill, Inc.

17. Touzi, R. and Lopes, A. (1996). Statistics of the Stokes Parameters and of the Complex Coherence Parameters in One-Look and Multilook Speckle Fields. *IEEE Trans. Geoscience and Remote Sensing*, **GRS-34**(2), 519–531.

18. Ender, J. H. G. (1999). Space-Time Processing for Multichannel Synthetic Aperture Radar. *IEE Electr. and Comm. Engineering J.*, pp. 29–38.

19. Anderson, T. W. (1984). An Introduction to Multivariate Statistical Analysis, 2 ed. John Wiley & Sons.

20. Muirhead, R.J. (1982). Aspects of Multivariate Statistical Theory, John Wiley & Sons.

21. Maiwald, D. and Kraus, D. (2000). Calculation of Moments of Complex Wishart and Complex Inverse Wishart Distributed Matrices. *IEE Proc.-Radar, Sonar Navig. (Pt. F)*, **147**(4), 162–168.

22. Grant, A. (2002). Rayleigh Fading Multi-Antenna Channels. *EURASIP Journal on Applied Signal Processing: Special Issue on Space-Time Coding and its Application (Part I)*, **JASP-02**(3), 316–329.

23. Golub, G. H. and Van Loan, C. F. (1989). Matrix Computations, Baltimore: Johns Hopkins University Press.

Annex A
Jacobian

The Jacobian associated with the change of variables

$$B_1 = \frac{A_{11} - \beta}{C_{11}}, \qquad B_2 = \frac{A_{22} - \beta}{C_{22}},$$

$$\eta = \frac{\alpha}{\sqrt{C_{11}C_{22}}} = \frac{\sqrt{\Re(A_{12})^2 + \Im(A_{12})^2}}{\sqrt{C_{11}C_{22}}}$$

and

$$\psi = \arctan\left(\frac{\Im(A_{12})}{\Re(A_{12})}\right),$$

is

$$\mathbf{J} = \begin{bmatrix} \frac{\partial B_1}{\partial A_{11}} & \frac{\partial B_1}{\partial A_{22}} & \frac{\partial B_1}{\partial \Re(A_{12})} & \frac{\partial B_1}{\partial \Im(A_{12})} \\ \frac{\partial B_2}{\partial A_{11}} & \frac{\partial B_2}{\partial A_{22}} & \frac{\partial B_2}{\partial \Re(A_{12})} & \frac{\partial B_2}{\partial \Im(A_{12})} \\ \frac{\partial \eta}{\partial A_{11}} & \frac{\partial \eta}{\partial A_{22}} & \frac{\partial \eta}{\partial \Re(A_{12})} & \frac{\partial \eta}{\partial \Im(A_{12})} \\ \frac{\partial \psi}{\partial A_{11}} & \frac{\partial \psi}{\partial A_{22}} & \frac{\partial \psi}{\partial \Re(A_{12})} & \frac{\partial \psi}{\partial \Im(A_{12})} \end{bmatrix} \tag{A.1}$$

$$= \begin{bmatrix} \frac{1}{C_{11}} & 0 & 0 & 0 \\ 0 & \frac{1}{C_{22}} & 0 & 0 \\ 0 & 0 & \frac{\Re(A_{12})}{\sqrt{\Re(A_{12})^2+\Im(A_{12})^2}\sqrt{C_{11}C_{22}}} & \frac{\Im(A_{12})}{\sqrt{\Re(A_{12})^2+\Im(A_{12})^2}\sqrt{C_{11}C_{22}}} \\ 0 & 0 & -\frac{\Im(A_{12})}{\Re(A_{12})^2+\Im(A_{12})^2} & \frac{\Re(A_{12})}{\Re(A_{12})^2+\Im(A_{12})^2} \end{bmatrix}.$$

Its determinant is

$$\det(\mathbf{J}) = \frac{1}{C_{11}C_{22}} \frac{1}{\sqrt{C_{11}C_{22}}\alpha} \tag{A.2}$$

or

$$\det(\mathbf{J}) = \frac{1}{C_{11}^2 C_{22}^2 \eta}. \tag{A.3}$$

Annex B
The Noncentral Complex Wishart Distribution

The noncentral Wishart distribution generalizes the noncentral χ^2 distribution in the same way the central Wishart distribution generalizes the χ^2 distribution; and the noncentral complex Wishart distribution is the extension of the noncentral Wishart distribution to the complex plane. The real Wishart distribution is discussed in detail in [19, 20]; the complex Wishart distribution was introduced in [10] and the inverse complex Wishart distribution in [21]. Although the complex noncentral case that we require is not difficult to develop, it is noticeably absent from the references above.

If the columns of the complex random matrix $\mathbf{Z} \in \mathbb{C}^{m \times n}$, i.e., the random vectors $\underline{Z}_k \in \mathbb{C}^{m \times 1}$ for $k = 1, \ldots, n$ are independent complex normal distributed $\mathcal{N}_m^{\mathbb{C}}(\underline{m}_k, \mathbf{R})$, then $\mathbf{A} = \mathbf{Z}\mathbf{Z}^H$ is said to have a complex noncentral Wishart distribution with n degrees of freedom, covariance matrix $\mathbf{R}$, and matrix of noncentrality parameters

$$\mathbf{\Omega} = \mathbf{R}^{-1}\mathbf{M}\mathbf{M}^H,$$

where $\mathbf{M} = [\underline{m}_1, \ldots, \underline{m}_n] \in \mathbb{C}^{m \times n}$. We will write that $\mathbf{A} \sim \mathcal{W}_m^{\mathbb{C}}(n, \mathbf{R}, \mathbf{\Omega})$.

When $n < m$, $\mathbf{A}$ is singular and the $\mathbf{A} \sim \mathcal{W}_m^{\mathbb{C}}(n, \mathbf{R}, \mathbf{\Omega})$ distribution does not have a density function. For $n > m$, the density function of $\mathbf{A}$ is given as

$$\begin{aligned} f_{\mathbf{A}}(\mathbf{A}) = \; & \frac{1}{\Gamma_m(n) \det(\mathbf{R})^n} \det(\mathbf{A})^{n-m} \exp(-\operatorname{tr}\mathbf{\Omega}) \\ & \cdot \exp\left(-\operatorname{tr}\left(\mathbf{R}^{-1}\mathbf{A}\right)\right) {}_0F_1(n; \mathbf{\Omega}\mathbf{R}^{-1}\mathbf{A}) \qquad \mathbf{A} > 0, \end{aligned} \tag{B.1}$$

where $\mathbf{\Omega} = \mathbf{R}^{-1}\mathbf{M}\mathbf{M}^H$ and $\Gamma_m(n) = \pi^{m(m-1)/2} \prod_{i=1}^{m} \Gamma(n - i + 1)$. ${}_0F_1(a; \mathbf{X})$ is the confluent hypergeometric function of matrix argument, which involves series of zonal polynomials. These functions have been defined for real variables in [20] and were extended for complex variables in [22].

Annex C
Generalized Bartlett's Theorem for the Noncentral Complex Wishart Distribution

C.1 Standard Normal Distribution

This subsection extents the generalized Bartlett's decomposition when the noncentrality matrix has rank one to the complex case. For real variables it is given in Theorem 10.3.8 of [20].

Let the columns of the complex random matrix $\mathbf{Z} \in \mathbb{C}^{m \times n}$, i.e., the random vectors $\underline{Z}_k \in \mathbb{C}^{m \times 1}$ for $k = 1, \ldots, n$ are identical complex normal distributed $\mathcal{N}_m^{\mathbb{C}}(\underline{m}, \mathbf{I})$ with $\underline{m} = [m_1, 0, \ldots, 0]^T$, so that $\mathbf{A} = \mathbf{Z}\mathbf{Z}^H$ is $\mathbf{A} \sim \mathcal{W}_m^{\mathbb{C}}(n, \mathbf{I}, \mathbf{\Omega})$ with $\mathbf{\Omega} = \operatorname{diag}(|m_1|^2, 0, \ldots, 0)$. Further, let the Cholesky decomposition of $\mathbf{A}$ be $\mathbf{A} = \mathbf{Q}\mathbf{Q}^H$, where the lower triangular matrix $\mathbf{Q}$ has real positive elements Q_{ii} on the diagonal. Then the elements Q_{ij} of $\mathbf{Q}$ are all statistically independent,

- $\frac{1}{2}Q_{11}^2$ is noncentral χ^2 distributed with $2n$ degrees of freedom and noncentrality parameter $|m_1|^2$, $\chi_{2n}^2(|m_1|^2)$,
- $\frac{1}{2}Q_{ii}^2$ for $i = 2, \ldots, m$ are central χ^2 distributed with $2(n-i+1)$ degrees of freedom, $\chi_{2(n-i+1)}^2$ and
- all off-diagonal elements Q_{ij} for $i \neq j$ are standard complex normal distributed, $\mathcal{N}^{\mathbb{C}}(0, 1)$.

Proof:

With $\mathbf{\Omega}$ having the above form, the density of $\mathbf{A}$ in eq. (B.1) is

$$f_{\mathbf{A}}(\mathbf{A}) = \frac{1}{\Gamma_m(n)} \det(\mathbf{A})^{n-m} \exp\left(-|m_1|^2\right) \exp(-\operatorname{tr}(\mathbf{A})) \; {}_0F_1(n; |m_1|^2 A_{11}).$$

Since $\mathbf{A} = \mathbf{Q}\mathbf{Q}^H$ we have

- $\operatorname{tr}(\mathbf{A}) = \operatorname{tr}\left(\mathbf{Q}^H\mathbf{Q}\right) = \sum_{j \leq i}^{m} Q_{ij}^* Q_{ij}$
- $\det(\mathbf{A}) = \prod_{i=1}^{m} Q_{ii}^2$ and $A_{11} = Q_{11}^2$.

The Jacobian is given as $\mathbf{J} = \prod_{i=1}^{m} Q_{ii}^{2(m-i+1)}$ [20], so that the joint density function of the Q_{ij} for $1 \leq i \leq j \leq m$ can be written as

$$\begin{aligned} f(\mathbf{Q}) = & \prod_{j<i}^{m} \frac{1}{\pi} \exp\left(-Q_{ij}^{*} Q_{ij}\right) \\ & \cdot \frac{1}{\Gamma(n)} Q_{11}^{n-1} \exp\left(-Q_{11}^{2}\right) \exp\left(-|m_1|^2\right) \; {}_0F_1(n; |m_1|^2 Q_{11}^{2}) \\ & \cdot \prod_{i=2}^{m} \frac{1}{\Gamma(n-i+1)} Q_{ii}^{n-i} \exp\left(-Q_{ii}^{2}\right), \end{aligned} \tag{C.1}$$

which is the product of the marginal density function for the elements of $\mathbf{Q}$ stated in the theorem.

C.2 Extension to General Case

Using the generalized eigenvalue decomposition for the hermitian-definite problem described, e.g., in [23] any arbitrary complex random matrix $\mathbf{Z}$ with independent $\mathcal{N}_m^{\mathbb{C}}(\underline{m}_i, \mathbf{R})$ distributed column vectors $\underline{Z}_i$ $(i = 1, \ldots, n)$ can be transformed into the form stated in the theorem C.1 as long as its matrix of expectation vectors $\mathbf{M} = [\underline{m}_1, \ldots, \underline{m}_n]$ has rank one. If

$$\mathbf{W} = \mathbf{R}^{-\frac{1}{2}} \mathbf{U},$$

where $\mathbf{U}$ are the eigenvectors of $\mathbf{R}^{-\frac{1}{2}} \mathbf{M}\mathbf{M}^H \mathbf{R}^{-\frac{1}{2}}$, i.e.,

$$\mathbf{R}^{-\frac{1}{2}} \mathbf{M}\mathbf{M}^H \mathbf{R}^{-\frac{1}{2}} = \mathbf{U}\mathbf{\Lambda}\mathbf{U}^H = \mathbf{U}\,\mathrm{diag}\,(\lambda, 0, \ldots, 0)\,\mathbf{U}^H, \tag{C.2}$$

(because $\mathbf{M}\mathbf{M}^H$ has rank one), then the random matrix

$$\mathbf{X} = \mathbf{W}^H \mathbf{Z}$$

has the expectation

$$\mathrm{E}\mathbf{X} = \mathbf{W}^H \mathbf{M}$$

with

$$\mathrm{E}\mathbf{X}\,\mathrm{E}\mathbf{X}^H = \mathbf{U}^H \mathbf{R}^{-\frac{1}{2}} \mathbf{M}\mathbf{M}^H \mathbf{R}^{-\frac{1}{2}} \mathbf{U} = \mathbf{\Lambda},$$

which follows from eq. (C.2). Now let

$$\mathbf{B} = \mathbf{X}\mathbf{X}^H = \mathbf{W}^H \mathbf{Z}\mathbf{Z}^H \mathbf{W} = \mathbf{W}^H \mathbf{A}\mathbf{W},$$

then

$$\begin{aligned} \mathrm{E}\mathbf{B} &= \mathbf{W}^H \mathrm{E}\mathbf{Z}\mathbf{Z}^H \mathbf{W} = \mathbf{W}^H \mathbf{R} \mathbf{W} \\ &= \mathbf{U}^H \mathbf{R}^{-\frac{1}{2}} \mathbf{R} \mathbf{R}^{-\frac{1}{2}} \mathbf{U} = \mathbf{U}\mathbf{U}^H = \mathbf{I}. \end{aligned}$$

Therefore, matrix $\mathbf{B}$ is $\mathcal{W}_m^{\mathbb{C}}\left(n, \mathbf{I}, \mathrm{diag}\left(\lambda, 0, \ldots, 0\right)\right)$ distributed with density

$$f(\mathbf{B}) = \frac{\det\left(\mathbf{B}\right)^{n-m}}{\Gamma_n(m)} \exp\left(-\operatorname{tr}\left(\mathbf{B}\right)\right) \exp\left(-\lambda\right) \; {}_0F_1(n; \lambda B_{11}) \tag{C.3}$$

where

$$B_{11} = \underline{u}_1^H \mathbf{R}^{-\frac{1}{2}} \mathbf{B} \mathbf{R}^{-\frac{1}{2}} \underline{u}_1 \tag{C.4}$$

and

$$\lambda = \underline{u}_1^H \mathbf{R}^{-\frac{1}{2}} \mathbf{M}\mathbf{M}^H \mathbf{R}^{-\frac{1}{2}} \underline{u}_1. \tag{C.5}$$

The vector $\underline{u}_1$ denotes the first eigenvector, i.e., the first column of $\mathbf{U}$.

DOCUMENT CONTROL DATA

(Security classification of title, body of abstract and indexing annotation must be entered when the overall document is classified)

1. ORIGINATOR (the name and address of the organization preparing the document. Organizations for whom the document was prepared, e.g. Establishment sponsoring a contractor's report, or tasking agency, are entered in section 8.)

DEFENCE RESEARCH & DEVELOPMENT CANADA - OTTAWA
DEPARTMENT OF NATIONAL DEFENCE
OTTAWA, ONTARIO, CANADA, K1A 0K2

2. SECURITY CLASSIFICATION (overall security classification of the document, including special warning terms if applicable)

UNCLASSIFIED

3. TITLE (the complete document title as indicated on the title page. Its classification should be indicated by the appropriate abbreviation (S,C or U) in parentheses after the title.)

Moving Target Detection with Along-Track SAR Interferometry (A Theoretical Analysis) (U)

4. AUTHORS (Last name, first name, middle initial)

GIERULL, CHRISTOPH, H.

5. DATE OF PUBLICATION (month and year of publication of document)	6a. NO. OF PAGES (total containing information. Include Annexes, Appendices, etc.)	6b. NO. OF REFS (total cited in document)
August 2002	55	23

7. DESCRIPTIVE NOTES (the category of the document, e.g. technical report, technical note or memorandum. If appropriate, enter the type of report, e.g. interim, progress, summary, annual or final. Give the inclusive dates when a specific reporting period is covered.)

DRDC Ottawa Technical Report

8. SPONSORING ACTIVITY (the name of the department project office or laboratory sponsoring the research and development. Include the address.)

DEFENCE RESEARCH & DEVELOPMENT CANADA - OTTAWA
DEPARTMENT OF NATIONAL DEFENCE
OTTAWA, ONTARIO, CANADA, K1A 0K2

9a. PROJECT OR GRANT NO. (if appropriate, the applicable research and development project or grant number under which the document was written. Please specify whether project or grant)	9b. CONTRACT NO. (if appropriate, the applicable number under which the document was written)
3DB29	

10a. ORIGINATOR'S DOCUMENT NUMBER (the official document number by which the document is identified by the originating activity. This number must be unique to this document.)	10b. OTHER DOCUMENT NOS. (Any other numbers which may be assigned this document either by the originator or by the sponsor)
DRDC Ottawa TR2002-084	

11. DOCUMENT AVAILABILITY (any limitations on further dissemination of the document, other than those imposed by security classification)

(X) Unlimited distribution
( ) Distribution limited to defence departments and defence contractors; further distribution only as approved
( ) Distribution limited to defence departments and Canadian defence contractors; further distribution only as approved
( ) Distribution limited to government departments and agencies; further distribution only as approved
( ) Distribution limited to defence departments; further distribution only as approved
( ) Other (please specify):

12. DOCUMENT ANNOUNCEMENT (any limitation to the bibliographic announcement of this document. This will normally correspond to the Document Availability (11). However, where further distribution (beyond the audience specified in 11) is possible, a wider announcement audience may be selected.)

13. ABSTRACT (a brief and factual summary of the document. It may also appear elsewhere in the body of the document itself. It is highly desirable that the abstract of classified documents be unclassified. Each paragraph of the abstract shall begin with an indication of the security classification of the information in the paragraph (unless the document itself is unclassified) represented as (S), (C), or (U). It is not necessary to include here abstracts in both official languages unless the text is bilingual).

(U) This technical report analyses, theoretically, the capability of ground moving target detection based on the SAR along-track interferometric phase. The probability density function of the interferometric phase is derived for the general case that moving target signals are superimposed upon the stationary clutter. This theoretical analysis is an extension of the known statistics for the clutter-only case. Several target models are proposed that depend on one hand on the spatial dimension of the moving target compared to the multilook resolution cell size, and on the other hand on the backscattering type, i.e., deterministic or random target signal. The derived density functions provide the means to quantify the performance limits (by determining the receiver operating characteristics) for any set of system and target parameters, such as false alarm rate, signal-to-clutter ratios (SCR) and target velocities. Hence, deeper insight is provided into results expected from upcoming SAR/GMTI systems such as the Radarsat2 Modex experiment or the enhanced airborne Aurora CP-140 SpotSAR system.

14. KEYWORDS, DESCRIPTORS or IDENTIFIERS (technically meaningful terms or short phrases that characterize a document and could be helpful in cataloguing the document. They should be selected so that no security classification is required. Identifiers such as equipment model designation, trade name, military project code name, geographic location may also be included. If possible keywords should be selected from a published thesaurus. e.g. Thesaurus of Engineering and Scientific Terms (TEST) and that thesaurus-identified. If it is not possible to select indexing terms which are Unclassified, the classification of each should be indicated as with the title.)

ALONG-TRACK INTERFEROMETRY
GROUND MOVING TARGET INDICATION
STATISTICS OF SAR INTERFEROGRAMS

Defence R&D Canada

Canada's leader in defence
and national security R&D

R & D pour la défense Canada

Chef de file au Canada en R & D
pour la défense et la sécurité nationale

www.drdc-rddc.gc.ca